

Article

Optimizing Ultra-High Vacuum Control in Electron Storage Rings Using Fuzzy Control and Estimation of Pumping Speed by Neural Networks with Molflow+

Soontaree Seangsri ¹, Thanasak Wanglomklang ², Nopparut Khaewnak ³, Nattawat Yachum ⁴
and Jiraphon Srisertpol ^{2,*} 

¹ Mechatronics Engineering Program, Institute of Engineering, Suranaree University of Technology, Nakhon Ratchasima 30000, Thailand

² School of Mechanical Engineering, Suranaree University of Technology, Nakhon Ratchasima 30000, Thailand

³ School of Mechatronics Engineering, Rajamangala University of Technology Tawan-ok, Chonburi 20110, Thailand

⁴ Synchrotron Light Research Institute, Nakhon Ratchasima 30000, Thailand

* Correspondence: jiraphon@sut.ac.th; Tel.: +66-4422-4412

Abstract: This paper presents the design of a fuzzy-controller-based ultra-high vacuum pressure control system and its performance evaluation for a sputter-ion vacuum pump used in the electron storage ring at the Synchrotron Light Research Institute (Public Organization) in Thailand. The production of synchrotron light requires advanced vacuum technology to maintain stability and prevent interference of electrons in an ultra-high vacuum pressure environment of about 10^{-9} Torr. The presence of heat and gas rupture from the pipe wall can affect the quality of the light in that area. The institute currently uses a sputter-ion vacuum pump which is costly and requires significant effort to quickly reduce pressure increases in the area. Maintaining stable vacuum pressure throughout electron motion is essential in order to ensure the quality of the light. This research demonstrates a procedure for evaluating the performance of a sputter-ion vacuum pump using a mathematical model generated by a neural network and Molflow+ software. The model is used to estimate the pumping speed of the vacuum pump and to design a fuzzy control system for the ultra-high vacuum system. The study also includes a leakage rate check for the vacuum system.

Keywords: ultra-high vacuum; sputter-ion vacuum pump; pumping speed; fuzzy; artificial neural network; Molflow+



Citation: Seangsri, S.; Wanglomklang, T.; Khaewnak, N.; Yachum, N.; Srisertpol, J. Optimizing Ultra-High Vacuum Control in Electron Storage Rings Using Fuzzy Control and Estimation of Pumping Speed by Neural Networks with Molflow+. *Systems* **2023**, *11*, 116. <https://doi.org/10.3390/systems11030116>

Academic Editors: Ed Pohl and Eric Specking

Received: 18 January 2023

Revised: 18 February 2023

Accepted: 21 February 2023

Published: 23 February 2023



Copyright: © 2023 by the authors. Licensee MDPI, Basel, Switzerland. This article is an open access article distributed under the terms and conditions of the Creative Commons Attribution (CC BY) license (<https://creativecommons.org/licenses/by/4.0/>).

1. Introduction

The Synchrotron Light Research Institute (Public Organization) is an institute that has a laboratory that provides services for the utilization of synchrotron light. Synchrotron light is generated by causing electrons to move at nearly the speed of light and forcing them to arc with a magnetic field, which causes the electrons to lose some energy and release energy in the form of electromagnetic waves. Synchrotron light has a high intensity and continuous energy value that covers four wavelengths, ranging from infrared to visible light, ultraviolet light, and X-rays, as shown in Figure 1.

The process of producing synchrotron light at the Siam Light Research Institute involves six main components: 1. an electron gun, 2. a linear accelerator (Linac), 3. a booster synchrotron, 4. a storage ring, 5. beamlines, and 6. an experimental station. The electron gun produces a large number of electrons, which are then divided into groups called electron bunches and accelerated in a straight line by microwave waves in the Linac. The booster synchrotron increases the energy of these electrons in a circle using radio waves, and the storage ring further accelerates the electrons to an energy of up to 1.2 GeV [1]. The beamlines bring the produced synchrotron light to the experimental station, where it

collides with a sample, and various scientific reactions occur. The data is then processed by scientists using a detector and a computer to analyze the atomic or molecular structure of the sample, as shown in Figure 2.

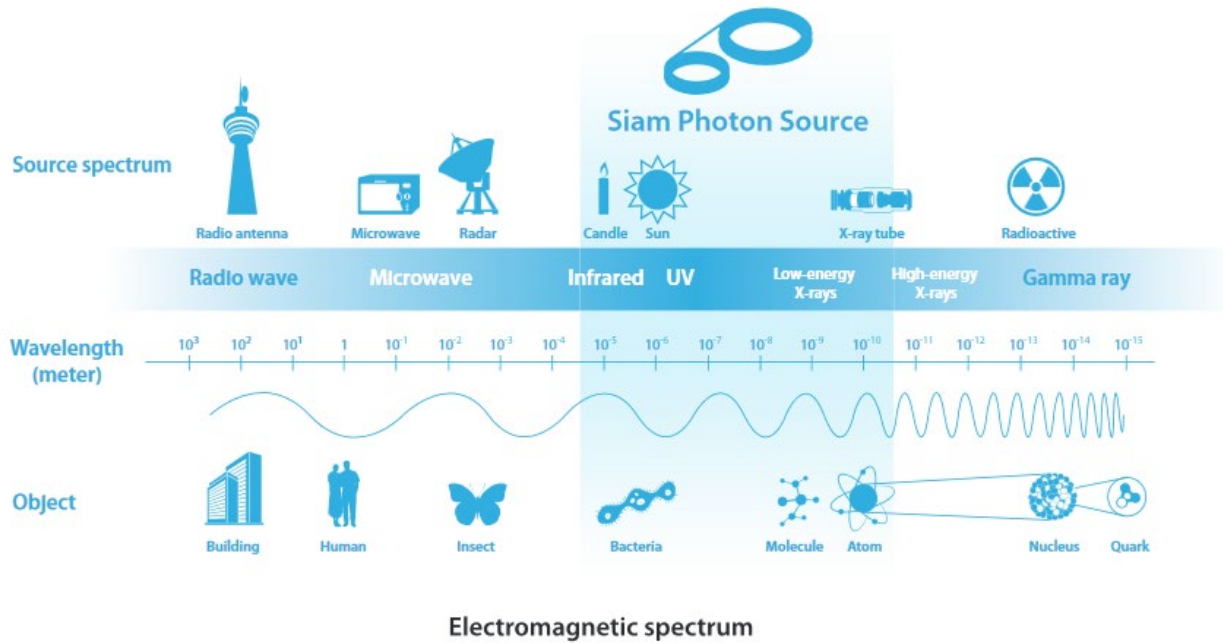


Figure 1. Properties of synchrotron light. Reference Source; https://www.slri.or.th/en_web/what-is-synchrotron-light.html (accessed on 1 January 2023).

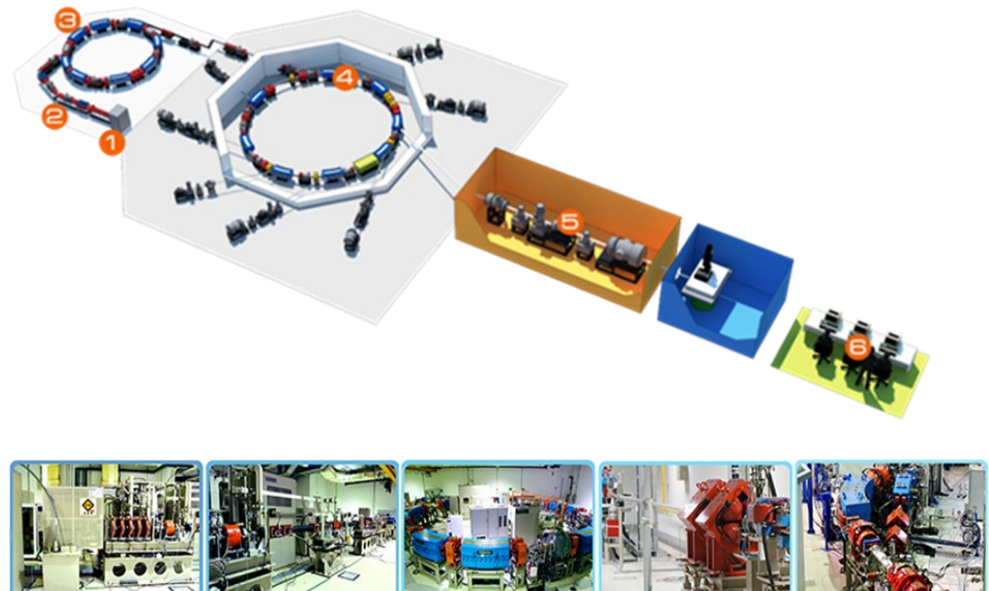


Figure 2. Synchrotron light generator. Reference Source; <http://www.slri.or.th/th/index.php/what-is-synchrotron-light/for-research.html> (accessed on 1 January 2023).

The production of synchrotron light requires advanced vacuum technology at a pressure of approximately 10^{-8} to 10^{-11} Torr in the beam in order to prevent interference, refraction, and collisions with air masses. Maintaining a constant ultra-high vacuum (UHV) pressure is essential to ensure the quality of the synchrotron light. Sputter-ion vacuum pumps are commonly used to maintain this pressure, but they are expensive and require a lot of work. Vacuum, created by vacuum pumps, refers to a space with low matter and pressure and is used in various applications such as research and industry. This paper

discusses the mathematical models of vacuum systems, pumps, measurement techniques, equipment installation, and testing processes. It also provides a guideline for selecting the right vacuum pump and briefly discusses support for optimum vacuum production [2–4]. The sputter pump, also known as an ion pump, was selected, and its characteristics were described [5]. This experiment used synchrotron light and required a UHV in the tube environment with gas loading analysis for the vacuum system chamber of the synchrotron radiation source 6 GeV (SR) [6]. Additionally, research on water absorption measurements at ultra-high and extreme-high vacuum was conducted [7]. A direct method for numerically calculating the pumping velocity of the sputter-ion pump was proposed [8], and the vacuum kinetic process of gas was also described. This paper also covers physical principles and modes of operation of vacuum pumps and vacuum meters, piping calculations, basics of gas composition measurement, leaks, and leak detection techniques [9–12]. The sputtered ion pump remains the unmatched pump for UHV, and research using Molflow+-based Monte Carlo particle test methods is performed to simulate UHV and synchrotron radiation calculations [13,14]. This paper also presents detailed designs and mechanical simulations of vacuum pump systems [15] to guide the design of this research. A number of research papers have proposed methods to improve optical quality in fields, such as physics and engineering, such as the measurement and analysis of high-resolution four-pole magnetic fields that focus on the electron beam [16]. In one study, the design and construction of an automatic control system for a 3-degree-of-freedom magnetic support for a synchrotron light generator, which aims to solve the problem of adjusting the magnet and electron transporter in the confinement ring to the correct level and position [17], was discussed. Another study described a linear electron acceleration system at an energy of 6 MeV that was developed to produce continuous and efficient X-rays, with the aim of maintaining stability in operation and tolerance to environmental changes by using a fuzzy algorithm and the Takagi–Sugeno inference method [18]. This research has proposed methods and approaches to improve the quality of synchrotron light, such as using a fuzzy algorithm in control systems. Fuzzy logic is a method of reasoning that allows for flexibility and complexity in problem-solving by using linguistic variables instead of numerical values. It is used in the area of fuzzy control, which formulates algorithms for control laws using logical rules [19]. This can be applied in a wide range of fields, such as control systems, artificial intelligence, and decision-making. Fuzzy logic, first introduced by Lotfi Zadeh in 1965, is widely used in embedded applications, particularly in small systems, robots, and machines [20]. It has various applications, such as fuzzy control, fuzzy signal processing, and fuzzy image processing [21]. Fuzzy logic is also widely used in PID control systems as a control algorithm and has been observed to perform better than traditional PID controllers in providing satisfactory control characteristics [22]. It can also be used in the process of liquid mixing in industries [23], as well as in creating a self-diagnostic system for a DC motor [24] and in optimizing a type-1 fuzzy controller for the Fault-Tolerant Control. Additionally [25], it can be applied in Negative Pressure Wound Therapy to improve the performance and safety of the treatment [26]. The goal of this research is to examine the application of fuzzy logic in controlling UHV conditions. Molflow+ is a Monte Carlo simulation software used to simulate pressure in particle accelerators [27]. It calculates theoretical pressure values using standard methods and can be used to design and analyze UHV systems [28]. The software can predict outgassing volume and pressure, estimate effective pumping speed [29], and determine the time needed to reach target pressure based on gas volume change. Molflow+ is mainly used for detailed 3D vacuum characterization in molecular flow systems [30]. Artificial neural networks (ANNs) have been widely applied in many fields for prediction purposes, including wind speed prediction, where the objective function is regression [31]. Feed-forward deep neural networks are also capable of achieving strong classification performance and have been shown to outperform shallow methods across diverse activity classes when optimized [32]. In the field of robot programming, the training results of neural network controllers have been presented, and the dynamic errors of different types of controllers have been analyzed [33]. Machine learn-

ing (ML), particularly deep learning techniques, have demonstrated efficacy in training, learning, analyzing, and modeling large complex structured and unstructured datasets [34]. However, when ML techniques are used for project duration prediction, the challenge is greater as each organization has a different dataset structure, features, and quality of data. To address this, a new dynamic ML tool based on an artificial neural network (ANN), which is automatically adapted and optimized to different types of prediction methods and different datasets, has been proposed [35]. The proposed decision-making system for leak detection is based on multiple generalized linear models and clustering techniques, which produces better recognition rates in comparison to a single model approach. Additionally [36], a physics-informed deep learning approach has been proposed for bearing fault detection, which consists of a simple threshold model and a deep convolutional neural network (CNN) model [37], which can reliably detect and classify four different bearing fault conditions [38]. All of these methods consider the design considerations, such as network architecture, performance, and implementation [39]. The objective of this article is to present a design for a UHV control system for a storage ring vacuum pipe using fuzzy control theory, and pumping speed estimation was estimated by Molflow+ in conjunction with ANN. The system aims to maintain a UHV level during electron beam movement. The results show that the UHV pressure can be controlled effectively. Additionally, using a method that estimates the pumping speed efficiency of the pump can aid in planning and making improvements, preventing damage, and ensuring efficient operation. The article is divided into five clear sections: Section 2: research methodology, experimental equipment, and system; Section 3: fuzzy control result and design for UHV, including the procedure for UHV pressure system and leak detection; Section 4: estimation of pump efficiency using a mathematical model generated from a neural network and Molflow+ software; and finally, Section 5: conclusions, where the findings are summarized.

2. Materials and Methods

2.1. Research Methodology

This research focuses readers on two main areas: controlling UHV pressure through fuzzy controller design and estimating the efficiency of pumping speed using an artificial neural network in conjunction with the Molflow+ program. The author will begin by describing the process of creating a vacuum pressure system [2,3], including procedures for leak detection in the experimental system. The design of the fuzzy controller will include the results of controlling pressure in the UHV system, which identifies the problem and determines the input and output variables that are involved. In this case, the input variable is the pressure reading from a sensor located at the center of the vacuum tube, and the output variables are the voltage supply to two independent ion vacuum pumps. For the input variables, triangle shape membership functions can be used. The output variables are defined by the singleton shape membership functions. We use the Mandani method to apply the membership functions. The center of the area can be used for the inference engine of the membership function output variables. Pressure data from the instrument at a steady state will be collected to simulate the outgassing rate of the experimental system with Molflow+ and then inputted into the learning process of the artificial neural network to create a model of the UHV system. The second part of this research will explain how this model is used to predict the pumping speed efficiency of the sputter-ion pump, as shown in Figure 3.

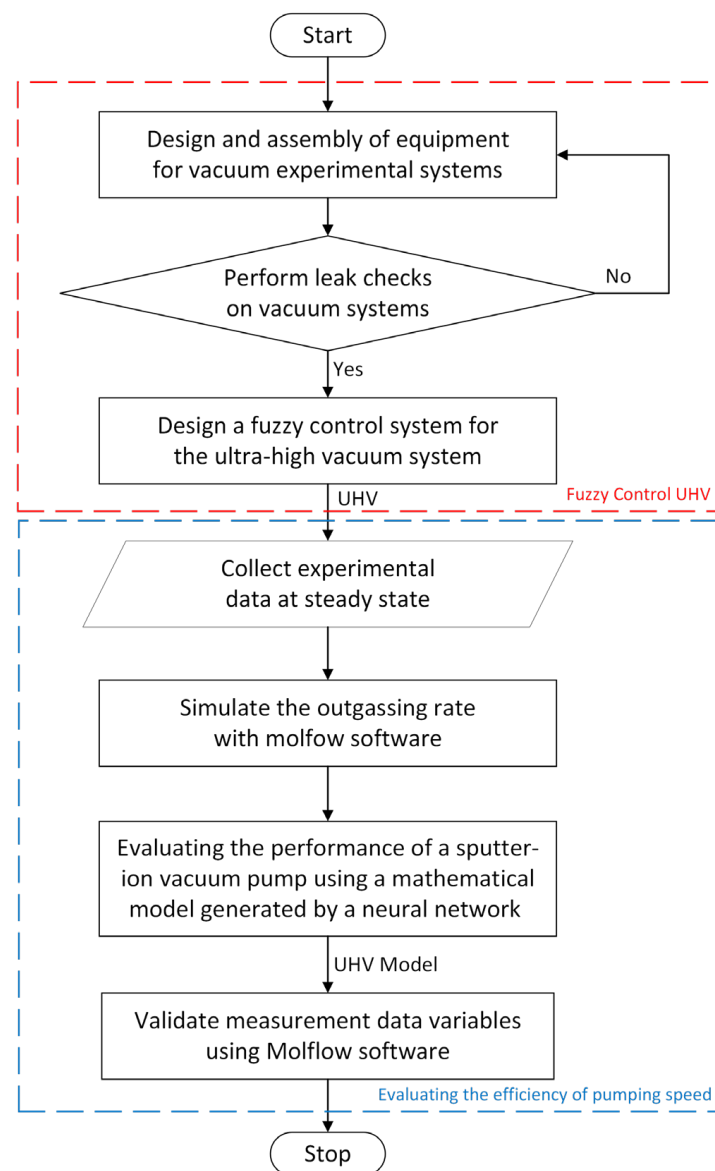


Figure 3. The Research Methodology.

A UHV pressure must be created in the pipeline using multiple vacuum pumps with different pressure ranges. A dry scroll pump, which has a spiral design and uses the twisting of the threads to create a pressure difference and move the air from the inside of the closed room to the outside atmosphere, can achieve a pressure of 10^{-2} Torr. A high molecular attractant pump can then be used to achieve a pressure of up to 10^{-8} Torr, and a sputter-ion pump, which captures gas molecules and sticks them in a confined area using a specific technique, can achieve a pressure of up to 10^{-12} Torr. Figure 4 illustrates the design of a standard pump. The system's equations are based on the assumption that the vacuum model conforms to Equations (1)–(5) [2–4]. The pressure P at an equilibrium state is expressed by Equation (1):

$$P = \frac{Q}{S}, \quad (1)$$

where Q is the net outgassing rate of the chamber under high vacuum. The net pumping speed of the pump varies with the pressure. The net outgassing rate of chamber Q also varies with the pressure.

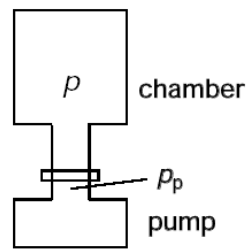


Figure 4. General Pump Structure. Reference Source; <http://www.most.go.th/main/th/109-knowledge/technology-integration/other-technologies/1366-vacuum-technology> (accessed on 1 October 2018).

The gas flow, including conductivity components within a vacuum (Conductance, C), and the pressure difference between vacuum volume joints can be represented by Equation (2):

$$Q = C(p - p_p) \quad (2)$$

Each flow in the vacuum pipeline is expressed by the continuity Equation (3):

$$Q = P_1 S_1 = P_2 S_2 \quad (3)$$

The relation between the pumping speed at the inlet of the pipeline (Schamber), at the outlet (S_{pump}), and the impedance (W) or conductance $C = 12 \frac{D^3}{L}$, diameter D (in cm), length L (in cm) of the pipeline has described the Equation (4):

$$S_{chamber} = \frac{1}{\frac{1}{S_{pump}} + W} = \frac{1}{\frac{1}{S_{pump}} + \frac{1}{C}} \quad (4)$$

The corresponding throughput Q (in torr. L/s), pressure P (in torr), pumping speed S (in L/s), and conductance C (L/s) are consequently given via Equation (5):

$$Q = C(P_{chamber} - P_{pump}) = S_{pump} P_{pump} = S_{chamber} P_{chamber} \quad (5)$$

2.2. Equipment

The vacuum experiment in this research was built using real-world materials supported by the Synchrotron Light Research Institute (Public Organization). The equipment includes a vacuum pressure system, a workpiece cleaning device, a control device, a leak detection device, and processing equipment. Further information regarding the numerical data is available in Figure 5 and Table 1, which provide detailed explanations of the experimental equipment.

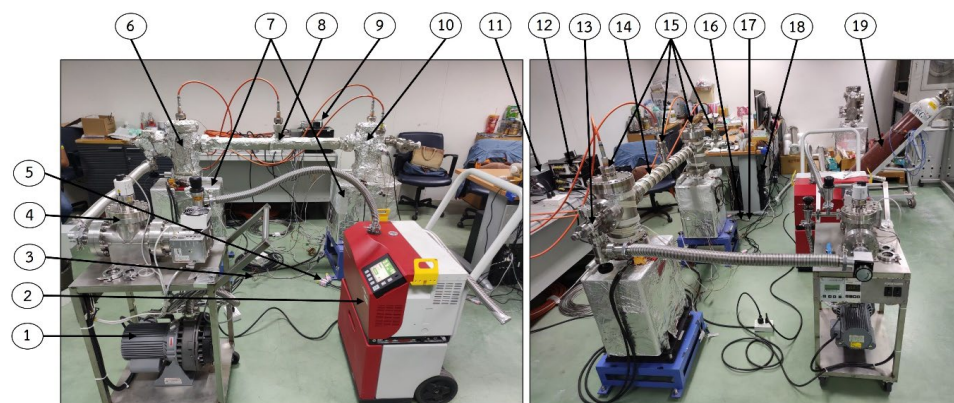


Figure 5. Ultra-high vacuum pressure system experimental equipment.

Table 1. Experimental equipment details.

No.	Name	Specification	Quantity
1	Scroll Vacuum Pump	- 0.4 kW, 50 Hz - 250 L/min (4.2 L/s), 1.2 ⁻² torr - 2.5 L/s helium pumping speed	1
2	Helium Leak Detector	- Minimum detectable leakage rate for helium 10 ⁻¹³ Pa m ³ /s	1
3	Thermocouple	- Type K	5
4	Turbo-Molecular Pump	- 1000 RPM, 0.4 A, 220 V	1
5	NI USB-TC01	- Type J, K, R, S, T, N, E and B thermocouple	5
6	Vacuum Chamber 1	- D = 146 mm, H = 310 mm	1
7	Sputter-Ion Pump	- Star cell, 500 L/s, typically 3–7 kV - pressures as low as 10 ⁻¹¹ mbar	2
8	Vacuum Pipe	- L = 1000 mm, D = 65 mm	1
9	Pfeiffer Vacuum TPG 300 Pressure Gauge	- Measures Pressure from Atmospheric Range, down to 10 ⁻¹¹ mbar - Pirani gauges/ Cold cathode gauges	2
10	Vacuum Chamber 2	- D = 146 mm, H = 285 mm	1
11	Sputter-Ion Pump Controller	- 2 Channels - Output 3000 V–7000 V	1
12	Baking Controller	- Max 10 A, 220 V - 304 stainless steel	2
13	All Metal Angle Valves	- Leak rate < 5–10 mbar.L/s - Temperature operating range from 450° C to –250° C	4
14	Heater	- V = 240 V, p = 170 W, L = 1.5 m - Bakeout temp ≤ 250 °C	5
15	Ionization Gauge	- Measuring range 5 × 10 ⁻³ to 1 × 10 ⁻¹¹ mbar	4
16	MOXA	- UPort 1110 V1.4.1, 5 VDC	3
17	RS-232		3
18	Computer	- Intel® Core™ i9-9900 CPU @3.1 GHz - RAM 32 GB, 64 bit	1
19	Helium Gas		1

2.3. Experimental System

The vacuum experimental system was designed to study UHV pressure and vacuum pressure control. It is divided into two systems: System 1, a vacuum chamber equipped with a sputter-ion pump with a pumping speed of 500 L/s and a pressure gauge installed in the position shown in Figure 6; and System 2, which consists of two vacuum chambers connected by a tube with a diameter of 65 mm and a length of 1000 mm. Both of these chambers are equipped with a sputter-ion pump with a pumping speed of 500 L/s and pressure gauges installed in 4 positions, as shown in Figure 7.

Figure 7 illustrates an experimental setup for a system consisting of two interconnected vacuum chambers. The chambers are connected by a 65 mm diameter tube that is 1000 mm in length. Sensor B is located at the center of the tube and measures the vacuum pressure at the highest point in the system. The first chamber has a diameter of 146 mm and a height of 310 mm, and sensor A is placed on the lid to measure the maximum pressure in that chamber. The second chamber has a diameter of 146 mm and a height of 285 mm; sensor C is located on top of its lid, measuring the maximum pressure in this chamber. Both chambers are equipped with sputter-ion pumps that have a pumping speed of 500 L/s and are located underneath each chamber. Additionally, sensor D is placed in the second chamber at the location indicated. The experimental system is exposed to a UHV pressure process, and the leakage rate of the system is monitored. Then, the system is sealed and ready to test the vacuum pressure control system and evaluate the performance of the sputter-ion pumps.

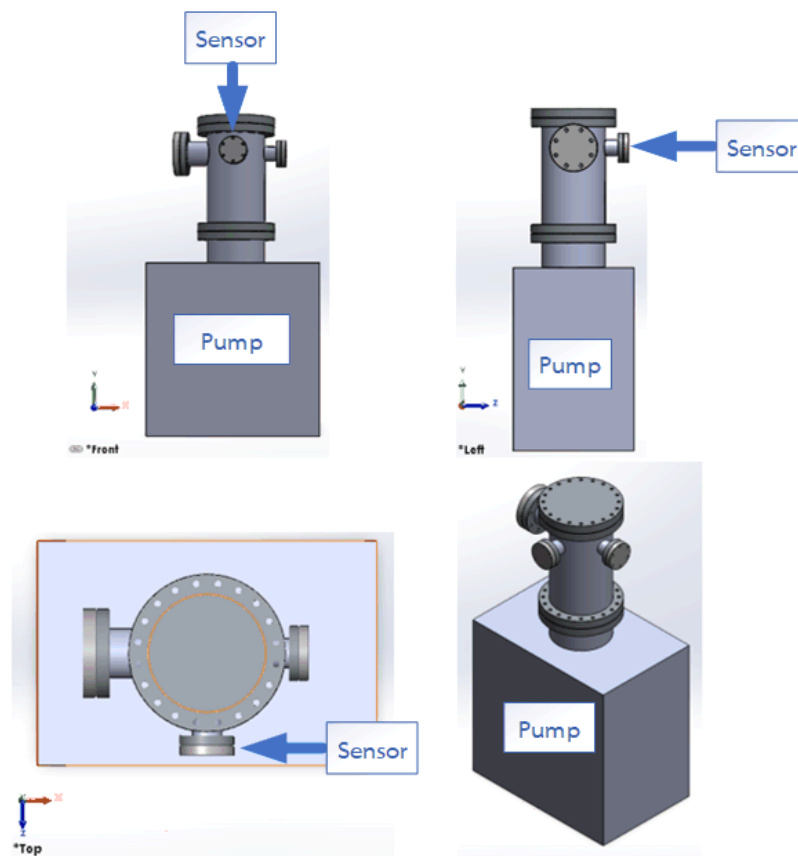


Figure 6. Illustrates the vacuum chamber for experimental system 1.

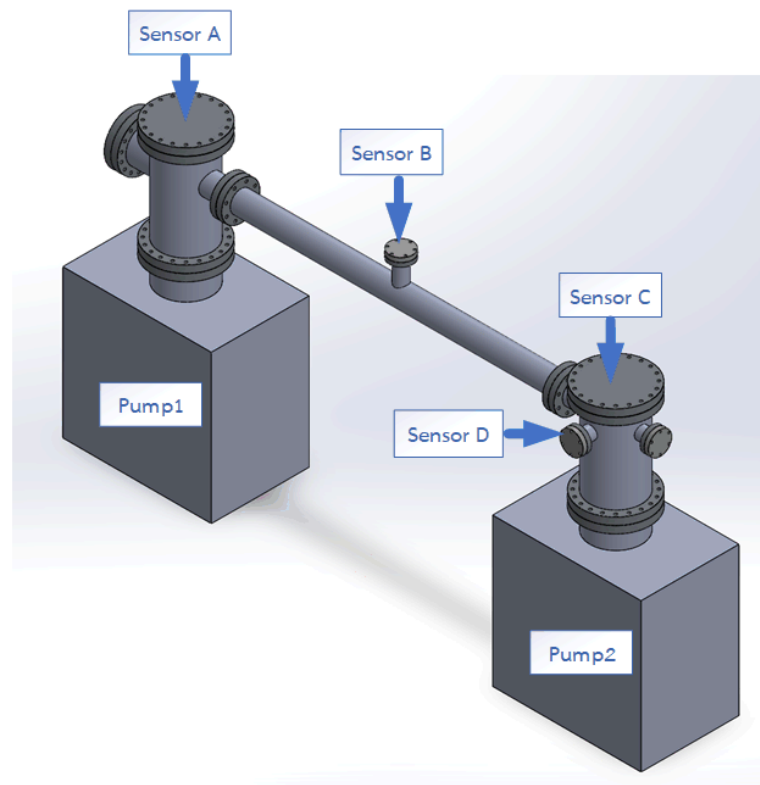


Figure 7. Illustrates the vacuum chamber for experimental system 2.

3. Ultra-High Vacuum by Fuzzy Control

Ultra-high vacuum (UHV) refers to a vacuum with a pressure level below 10^{-9} Torr. Fuzzy control is a method of controlling systems using fuzzy logic, which is a mathematical tool for representing and manipulating uncertain or imprecise information. In a fuzzy control system, the inputs and outputs are mapped to fuzzy sets, and a set of fuzzy rules are used to determine the control actions. Using fuzzy control for UHV systems allows for the system to adapt to changing conditions and make decisions based on imprecise or uncertain information. This can improve the stability and efficiency of the system and also increase its robustness against disturbances and uncertainties. This section discusses the process of designing and constructing the UHV systems. It covers implementing leak detection and a fuzzy controller design for UHV, including the results of the fuzzy pressure control.

3.1. Procedure for Ultra-High Vacuum Pressure System

Figure 8 illustrates the process for creating a UHV pressure system for this research. The process begins by cleaning the workpiece (vacuum chamber) with ethanol to prepare it for the UHV pressure process. To achieve UHV pressure, the pressure must be gradually increased from atmospheric pressure to a value of 10^{-1} to 10^{-2} Torr using dry scroll vacuum pumps and then to a pressure of 10^{-2} to 10^{-7} Torr using a turbo pump and a molecular pump. The workpiece is then outgassed at a temperature of about 120 degrees Celsius for at least 3 days. Before and after heating, a leak test is performed on the workpiece by spraying helium gas outside the workpiece at suspected leakage points, such as along flange joints in vacuum chamber connections and pipes. The CF (Con Flat) flange uses a copper gasket with high thermal conductivity and metal circumferential prongs. The soft properties of the copper gasket allow for a very tight seal between the two metal flanges by distorting the gasket. CF flanges can operate at a pressure of about 10^{-13} Torr. If a leak is detected, helium gas will seep through the leak and into the workpiece, where it will be detected by the helium leak detector. If no leak is found, the process continues by using a sputter-ion pump until the vacuum pressure reaches a level of 10^{-8} Torr and can no longer be increased. The valve between the vacuum chamber, the dry scroll pump, and the high molecular attractant pump operating system is then closed, allowing the system to be evacuated using only a sputter-ion pump. Later, we designed a fuzzy controller to command the sputter-ion pump controller to maintain the vacuum pressure through a LabVIEW program connected to a computer via RS-232 and a MOXA module. The definition of each pressure range is described in Table 2.

Table 2. Shows the Range of Vacuum Pressure [40].

Range of Vacuum Pressure	Minimum Pressure (Torr)	Maximum Pressure (Torr)
Low Vacuum (LV)	2.5×10	7.5×10^2
Medium Vacuum (MV)	7.5×10^{-4}	2.5×10
High Vacuum (HV)	7.5×10^{-7}	7.5×10^{-4}
Very High Vacuum (VHV)	7.5×10^{-10}	7.5×10^{-7}
Ultra-High Vacuum (UHV)	7.5×10^{-13}	7.5×10^{-10}
Extreme-High Vacuum (XHV)		$\leq 7.5 \times 10^{-13}$

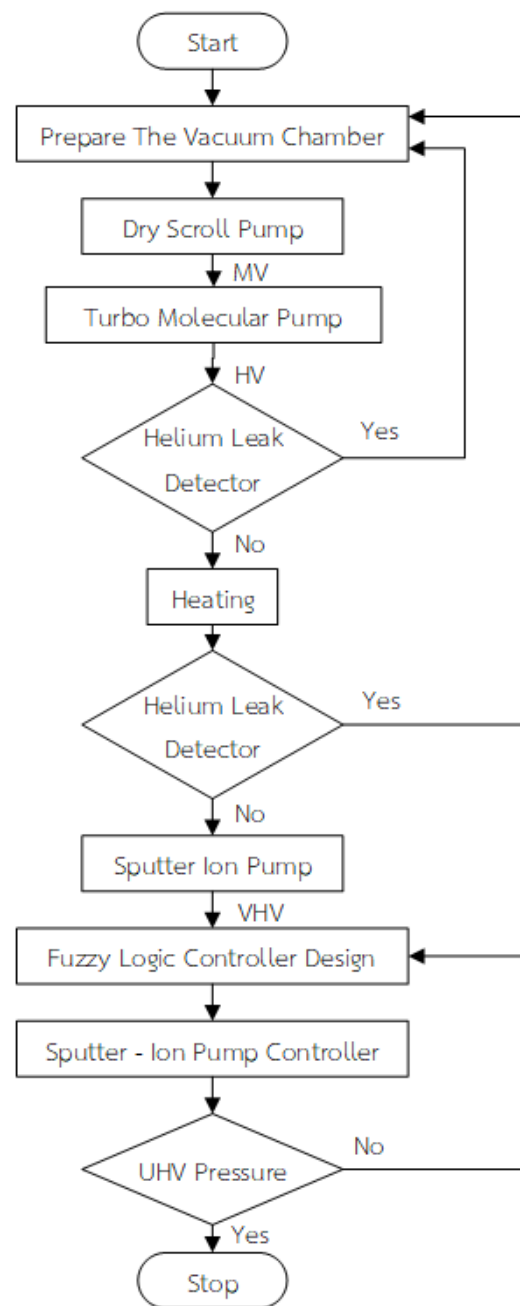


Figure 8. Ultra-high vacuum pressure process.

3.2. Procedure for Checking for Leaks in the Vacuum System

Vacuum leak testing is an essential step in the vacuum-making process. The process involves achieving a system vacuum of 10^{-6} Torr using dry scroll vacuum pumps in combination with a Turbo Molecular pump and then bringing in helium gas to spray outside the workpiece at suspected leak points. If a leak is detected, the helium gas will seep through the leak and into the workpiece, where it will be detected by the helium leak detector [11]. The leak inspection is performed from top to bottom as the helium gas rises to higher altitudes (as shown in Figure 9). After the inspection, if no leakage points are found, a sputter-ion pump is used to maintain the vacuum pressure at 10^{-8} Torr. In this method, a known amount of helium gas is introduced into the system, and the presence of helium is used to identify any leaks that may be present. Finally, leak testing is important to ensure the integrity and performance of UHV systems.



Figure 9. Checking for leaks in the vacuum system.

3.3. Sputter-Ion Pump

The working of a sputter-ion pump is based on the supply voltage provided to it. The supply voltage ranges from 3000, 5000, and 7000 volts and is related to the vacuum pressure value, as shown in Figure 10. The graph shows that the start of the sputter-ion pump starts from the low vacuum pressure value on the right side of the sputter-ion pump. A supply voltage of 7000 volts provides maximum pump efficiency, while a supply voltage of 5000 volts provides optimal pumping efficiency when the vacuum pressure is increased to a pressure of 1×10^{-7} mbar. When the system has a vacuum pressure of 5×10^{-9} mbar, the supply voltage for the sputter-ion pump at 3000 volts provides optimal pumping efficiency. This can be explained in Table 3.

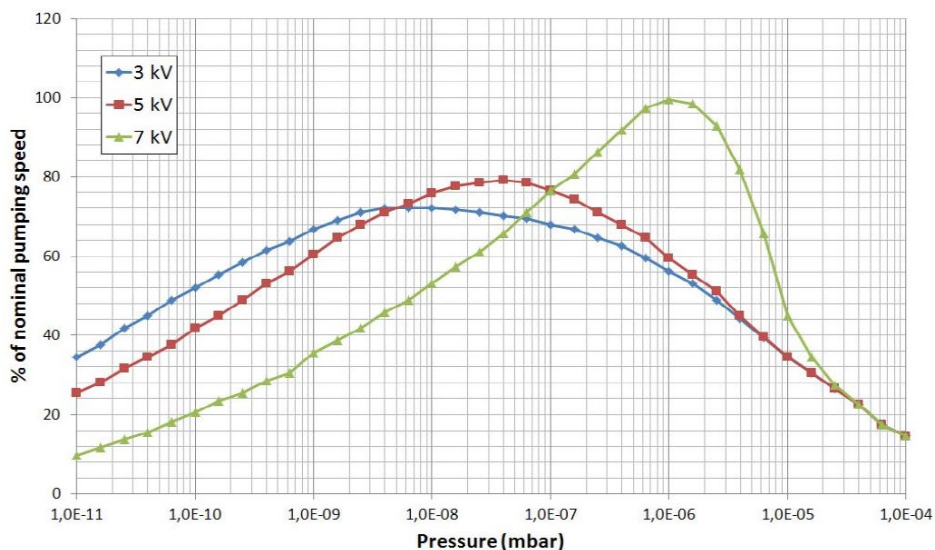


Figure 10. Shows the relationship between the % of nominal pumping speed and the pressure values of 3000, 5000, and 7000 Volt at different vacuum pressures of the Controller of Ion Pump. Reference Source; ION Pumps for UHV Systems; Synchrotrons and Particle Accelerators.

Table 3. The pumping speed relationship equation at 3000 V, 5000 V, and 7000 V supply voltages.

V	Equation (Mbar)	R ²	Pumping Speed		Pchamber	
			(%)	L/s	P (Mbar)	P (Torr)
3000	$y = 5.525\ln(x) + 179.91$	0.9733	48–72	240–360	6×10^{-11} – 5×10^{-9}	4.5×10^{-11} – 3.75×10^{-9}
5000	$y = 4 \times 10^{22}x^3 - 9 \times 10^{15}x^2 + 5 \times 10^8x + 71.053$	0.9044	72–76	360–380	5×10^{-9} – 1×10^{-7}	3.75×10^{-9} – 7.5×10^{-8}
7000	$y = 10.52\ln(x) + 246.07$	0.9816	76–99	380–495	1×10^{-7} – 1×10^{-6}	7.5×10^{-8} – 7.5×10^{-7}

In this research, an ion pump of 500 L/s was selected. The goal of this research is to develop the ability to adjust the voltage supplied to the sputter-ion pump to be more precise. The voltage will be supplied at 3000, 4000, 5000, 6000, and 7000 volts to optimize the pumping speed of the pump at each vacuum pressure range, where the 4000 and 6000 volts are comparable estimates from the pump specification, as shown in Table 4.

Table 4. The relationship equation between pumping speed at 3000, 4000, 5000, 6000, and 7000 volts to the vacuum pressure.

V	Equation (Mbar)	R ²	Pumping Speed (%)	Controller	
				P (Mbar)	P (Torr)
3000	$y = 4.3486\ln(x) + 156.73$	0.9732	64–72	6.2×10^{-10} – 5×10^{-9}	4.65×10^{-10} – 3.75×10^{-9}
4000	$y = 8 \times 10^8x + 68.048$	0.9973	72–76	5×10^{-9} – 1×10^{-8}	3.75×10^{-9} – 7.5×10^{-9}
5000	$y = 2.1615\ln(x) + 115.97$	0.9709	76–79	1×10^{-8} – 4×10^{-8}	7.5×10^{-9} – 3×10^{-8}
6000	$y = 4.5108\ln(x) + 155.92$	0.9784	79–83.5	4×10^{-8} – 2×10^{-7}	3×10^{-8} – 1.5×10^{-7}
7000	$y = 10.52\ln(x) + 246.07$	0.9816	83.5–99	2×10^{-7} – 1×10^{-6}	1.5×10^{-7} – 7.5×10^{-7}

The relationship between the vacuum pressure value and the pumping speed efficiency of the sputter-ion pump generated in Table 4 shows the voltage supply range that achieves the pumping speed efficiency of the pump suitable for each vacuum pressure value range. The low vacuum pressure range, such as 1.5×10^{-7} – 7.5×10^{-7} Torr, is suitable for supplying voltage at 7000 volts, which will get the pumping speed of the pump at 83.5–99 percent of the pump performance of 500 L/s. This research aims to establish a fuzzy law for controlling the action mechanism or the change of supply voltage of the ion pump based on the relations in Table 4.

3.4. Fuzzy Design

Fuzzy logic is a method of reasoning that resembles human reasoning. The most basic concept in fuzzy logic is the fuzzy set. A fuzzy set is a set that has a degree of membership between 0 and 1 rather than the traditional binary (true/false) membership of a standard set. This degree of membership indicates the extent to which an element belongs to the set. It is particularly useful in situations where precise mathematical models are unavailable or impractical and can be used to make decisions and control processes.

The application of fuzzy logic control in UHV systems is used to maintain a desired vacuum pressure of less than 3.75×10^{-9} torr. The control system employs a Single-Input-Multiple-Output (SIMO) fuzzy controller, where the input is the pressure reading from a sensor located at the center of the vacuum tube, and the outputs control the voltage supply to two independent ion vacuum pumps. The fuzzy input variable is the pressure reading from sensor B, and the member function consists of a fuzzy set of five language variables {N, SN, Z, SP, P}. The output variables are the voltages fed to the first and second ion vacuum pumps, consisting of language variables {L, SL, M, SH, H} and {L2, SL2, M2, SH2, H2}, respectively, as defined in Table 5.

Table 5. Fuzzy control design to maintain vacuum pressure.

No.	Pressure Input (Torr)	Input Variable	Output Variable 1	Output Variable 2	Percent Variable	Voltage Supply 1	Voltage Supply 2
1	$\leq 3.75 \times 10^{-9}$	N	L	L2	0	3000	3000
2	$3.751 \times 10^{-9} - 7.5 \times 10^{-9}$	SN	SL	SL2	25	4000	4000
3	$7.51 \times 10^{-9} - 3 \times 10^{-8}$	Z	M	M2	50	5000	5000
4	$3.01 \times 10^{-8} - 1.506 \times 10^{-7}$	SP	SH	SH2	75	6000	
5	$\geq 1.507 \times 10^{-7}$	P	H	H2	100	7000	7000

The input and output parameters of the Fuzzy Rules in Table 5 can be generated and applied using a LabVIEW program connected to a 4UHV ion pump controller for a voltage regulator that powers an ion vacuum pump via an RS232 cable and a MOXA module. This allows the system to be operated in real time by a computer. Figure 11 demonstrates the input and output variable assignments of fuzzy rules for fuzzification using LabVIEW software (LabVIEW 2016, License No. M76X33883, Synchrotron Light Research Institute, Thailand), and Figure 12 shows the calculation of fuzzy inference using a fuzzy rule whose principle is “if input, then output” in the diagnostic process, which is analyzed and processed according to specified conditions with the LabVIEW software. These rules are used to map input variables to output variables by using fuzzy membership functions. These functions are used to assign a degree of membership to each input value, which is then used to generate the output value.

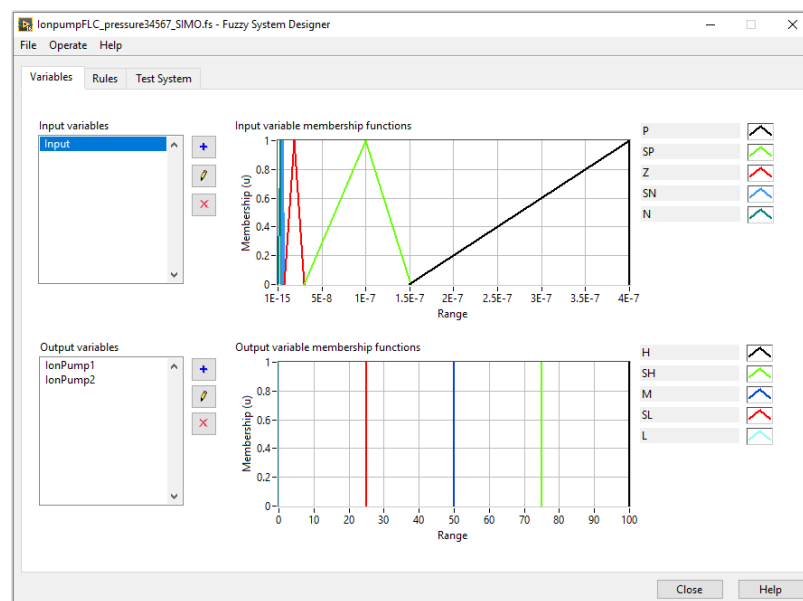


Figure 11. Configure inputs and outputs of the fuzzy rule.

Figure 13 shows the simulation of the generated fuzzy rule. The defuzzification converts the language obtained in the form of fuzzy inference into a single true output value from a five-member fuzzy set {0, 25, 50, 75, 100} percent instead of supplying pressure at {3000, 4000, 5000, 6000, 7000} volts, respectively, by Figure 13a,b when the input pressures are 9×10^{-14} Torr and 3.75×10^{-9} Torr, respectively. That is to say that when the input pressure value is less than or equal to 3.75×10^{-9} Torr, with the input linguistic value N, it will enter the first rule to get the output of the first pump, and the second has a linguistic variable value of L and L2, respectively, representing 0 percent output where the supply voltage is 3000 Volt.

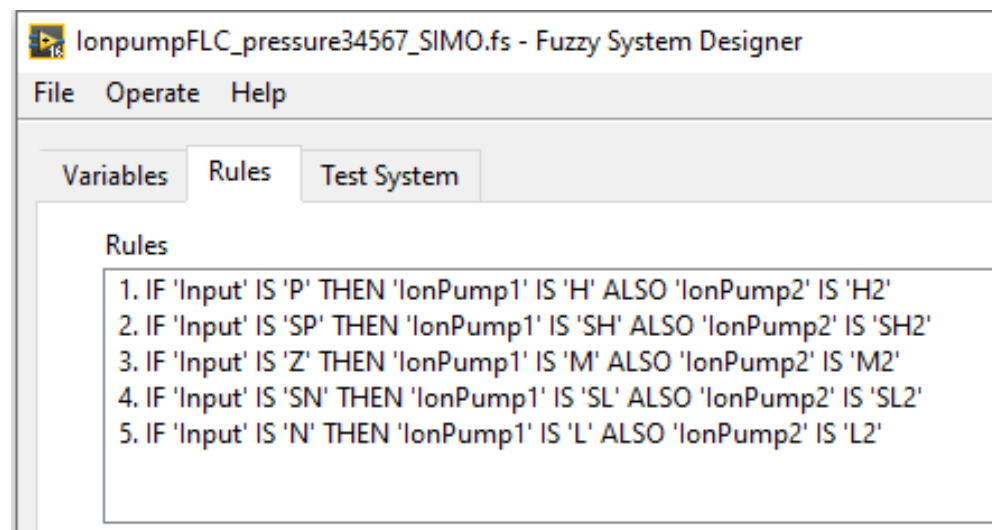
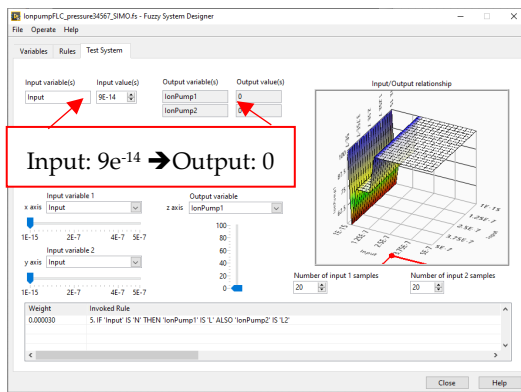


Figure 12. Fuzzy rules to control pressure values via LabVIEW software.

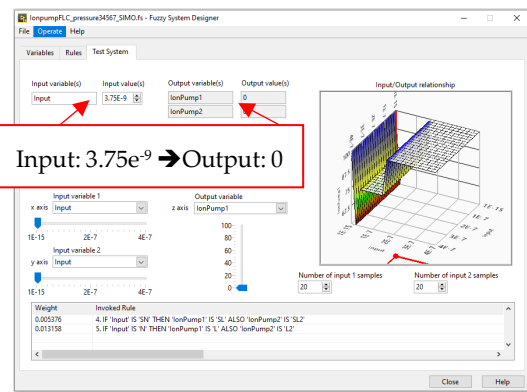
While Figure 13c,d shows the input pressure is 3.76×10^{-9} Torr and 7.5×10^{-9} Torr, respectively, which enters the second rule, with the linguistic variable of the input SN, the output of the first pump and the second pump with the linguistic variable is SL and SL2, respectively, representing 25 percent of the output where the supply voltage is 4000 Volt. Similarly, Figure 13e,f shows the input pressure values of 7.51×10^{-9} Torr and 3×10^{-8} Torr, respectively, which enter Rule 3, with the linguistic variable of the input Z, the output of the first pump and the second pump with the linguistic variable of M and M2, respectively, representing 50 percent of the output. The input pressure is 3.01×10^{-8} Torr and 1.506×10^{-7} Torr, respectively. Rule 4 with the linguistic variable of the input SP, the output of the first pump, and the second pump with the linguistic variable of SH, SH2, respectively, representing 75 percent output, as shown in Figure 13g,h, where the voltage is supplied at 6000 Volt, and Figure 13i,j shows the input pressure values of 1.507×10^{-7} Torr and 5×10^{-5} Torr, respectively, which enters the law of 5 with the input linguistic variable P; the output of pump 1 and 2 is linguistic variable H, H2 respectively, representing 100 percent output, which will supply voltage at level 7000 Volt.

Fuzzy Pressure Control Improves Test System Performance

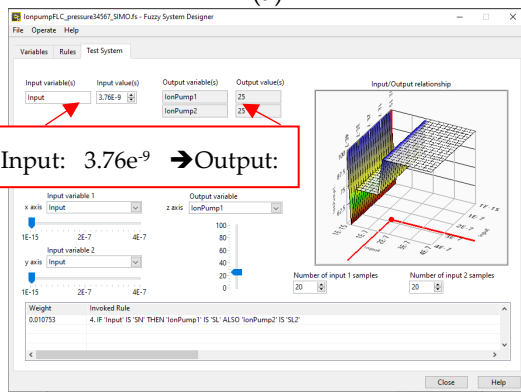
Table 5 establishes fuzzy rules that were tested on System 1, which is a vacuum chamber connected to a vacuum pump. Figure 14 illustrates the hardware used for testing and demonstrates how the fuzzy rule controls the voltage power supply to maintain pressure in the vacuum chamber. Figure 15 shows the supply voltage to the sputter-ion vacuum pump with 3000, 4000, 5000, 6000, and 7000 volts, respectively, (left y-axis) in relation to the vacuum chamber pressure at the location where the pressure value is to be controlled. It is clearly divided by the fuzzy rule range with a dotted line (right y-axis). It can be seen that the pressure change follows the properly designed fuzzy rule. That is when the vacuum chamber pressure is lower than 3.75×10^{-9} Torr, the pump supply voltage is 3000 volts, and 4000 volts is supplied if the vacuum chamber pressure is 3.75×10^{-9} Torr and is in the range of 3.751×10^{-9} – 7.5×10^{-9} Torr. When the vacuum chamber pressure increases in the range of 7.51×10^{-9} – 3×10^{-8} Torr, the pump supply voltage is 5000 volts. When the vacuum chamber pressure increases in the range of 3.01×10^{-8} – 1.506×10^{-7} Torr, the pump supply voltage is 6000 volts. If the pressure is greater, the pump supply voltage is 7000 volts.



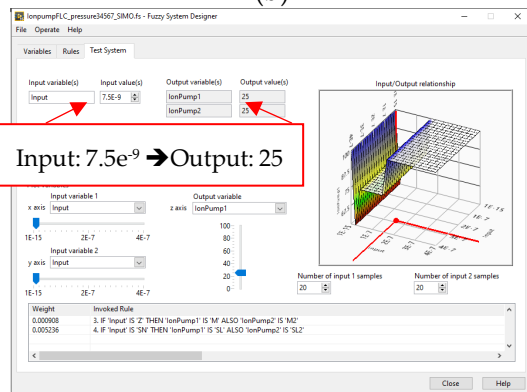
(a)



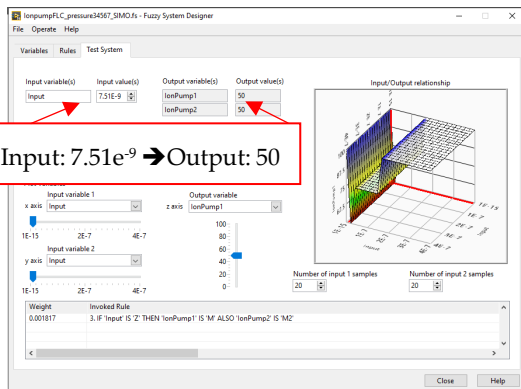
(b)



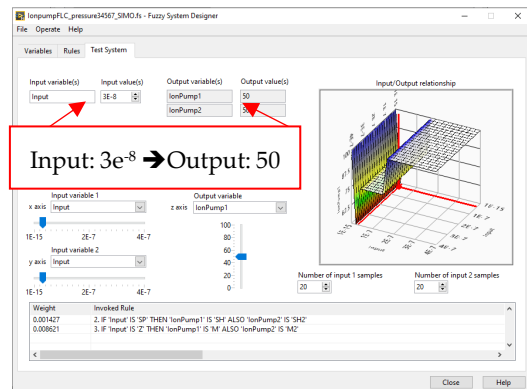
(c)



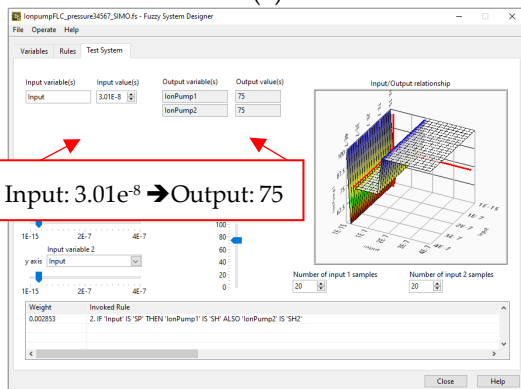
(d)



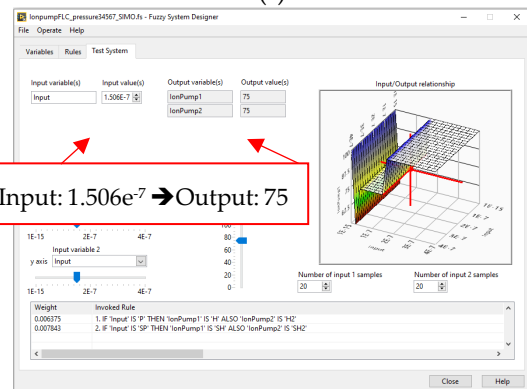
(e)



(f)



(g)



(h)

Figure 13. Cont.

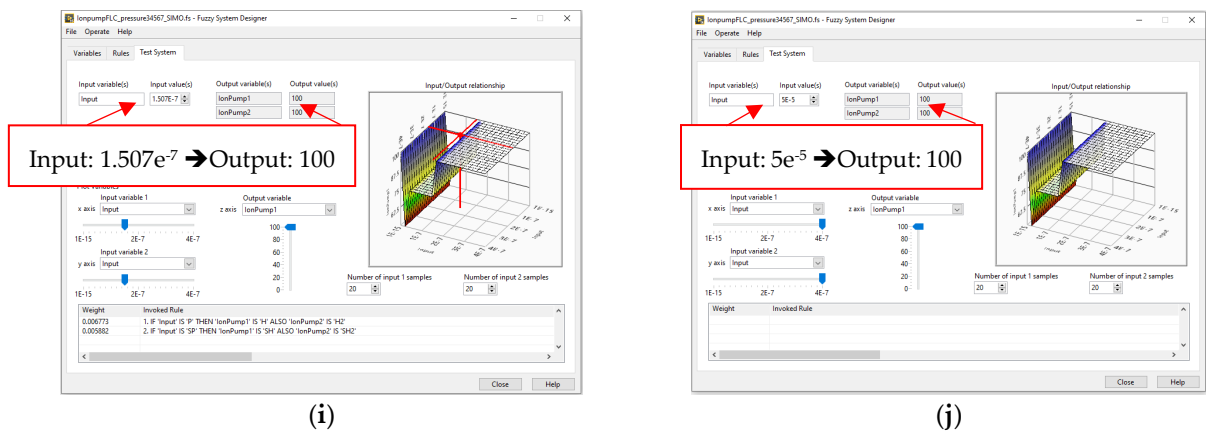


Figure 13. The simulation of the generated fuzzy rule. (a) minimum rule 1; (b) maximum rule 1; (c) minimum rule 2; (d) maximum rule 2; (e) minimum rule 3; (f) maximum rule 3; (g) minimum rule 4; (h) maximum rule 4; (i) minimum rule 5; and (j) maximum rule 5.



Figure 14. Hardware installed for system 1.

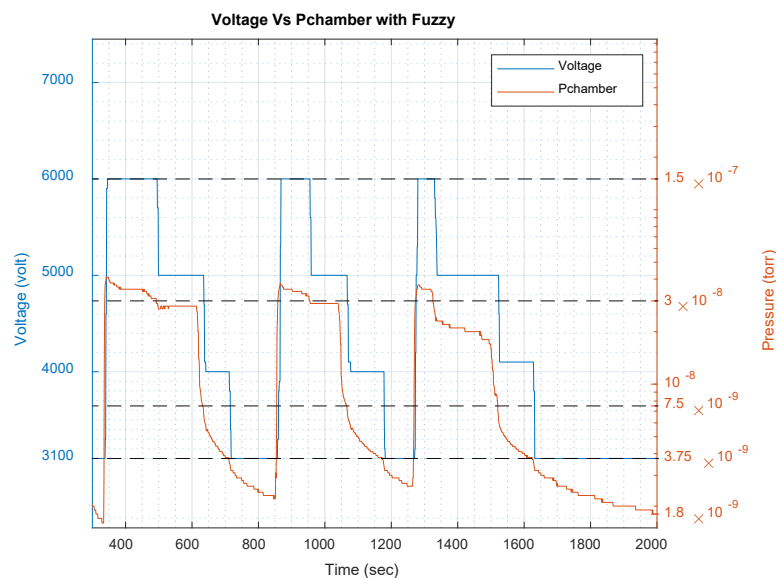


Figure 15. Show how fuzzy rules work for system 1.

When the pressure control characteristics of the vacuum chamber 1 system are known, they can be applied to a two-chamber system using the same fuzzy rules established in Table 5. The behavior is that the vacuum pressure value at the middle position of the pipe connecting the vacuum chambers is used as the pressure value for the control. This is because the pressure value at this position is the highest in the system. If the pressure value at this position is in control, the pressure value at any other location will be within the range of the UHV pressure value. The regulating pressure is achieved when the two sputter-ion vacuum pumps operate according to the established fuzzy rules. The equipment used to test this system is shown in Figure 16. The control results can be seen in Figure 17 and expanded for clarity in Figure 18. These figures demonstrate that the vacuum pressure at the center of the pipe, which is the position of the maximum pressure, can be controlled to be below 3.75×10^{-9} torr.

The real test results revealed the efficacy of fuzzy pressure control in optimizing the performance of the system. Fuzzy logic is used to regulate the supply voltage of the sputter-ion pump to achieve different pumping speeds at the same pressure for various voltage levels. This allows for better control over the pumping process and ensures that the optimal pumping speed is maintained for the given pressure conditions. Fuzzy logic can be useful for controlling various processes in UHV systems. In UHV systems, it is important to maintain a very low-pressure environment to prevent contamination or interference with the experiment or process being performed. Fuzzy logic can be used to control the parameters that affect the pressure inside the UHV system, such as the flow rates of gases, the temperature of the system, or the speed of vacuum pumps. By adjusting these parameters using fuzzy logic, it is possible to achieve the desired pressure conditions while minimizing energy consumption and maintaining stability. In a system that does not have fuzzy logic, controlling the various parameters and components of a UHV system can be more challenging. Without a fuzzy logic controller, the system may rely on conventional control methods, such as PID (proportional-integral-derivative) control or on-off control. Conventional control methods can be effective in maintaining a set point for a given parameter, such as pressure or temperature, but they may not be able to handle the complexity of UHV systems, which often involve multiple parameters and interactions between components. For example, in a UHV system with multiple vacuum pumps, conventional control methods may not be able to optimize the pumping speed of each pump to achieve the desired pressure conditions. This can lead to inefficient operation, longer process times, or decreased product quality. In addition, conventional control methods may not be able to adapt to changing conditions or non-linear behavior in the system. This can even cause instability in the system. Overall, the use of fuzzy logic in UHV systems provides a more flexible and adaptive approach to control, allowing the system to respond to changing conditions and optimize performance in real time. Fuzzy logic can also handle complex systems with multiple parameters and components, making it a more effective control method for UHV systems. From the above experiments, the vacuum pressure at the location where the measuring instrument is installed is known, as well as the voltage supplied to the sputter-ion vacuum pump. However, the outgassing rate of the system is unknown, and more importantly, the efficiency of the pump in pumping is unknown. This is because the pump has a long service life, and through heavy use, there may be some factors that reduce the pumping efficiency, resulting in a decrease in pumping speed. Therefore, this research has studied the behavior of the vacuum pressure profile in the experimental system using the Molflow+ software application, starting with the experimental system 1 vacuum chamber. This will allow for a better understanding of the characteristics and behavior of the vacuum pressure, which will be discussed in the next section.

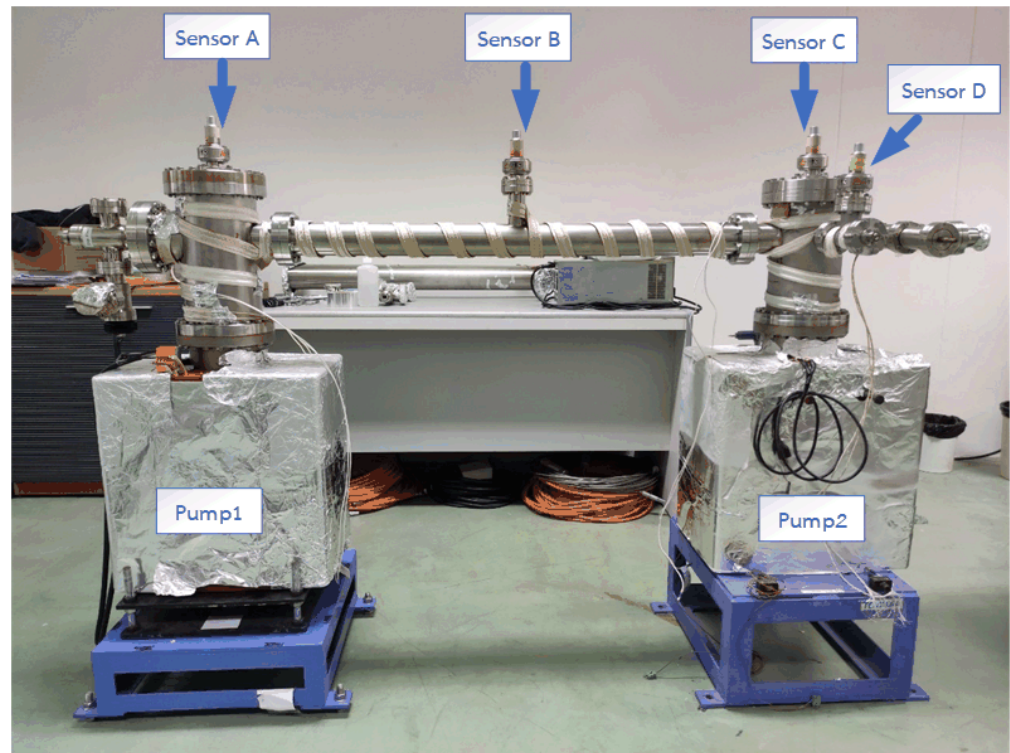


Figure 16. The equipment used to test this system 2.

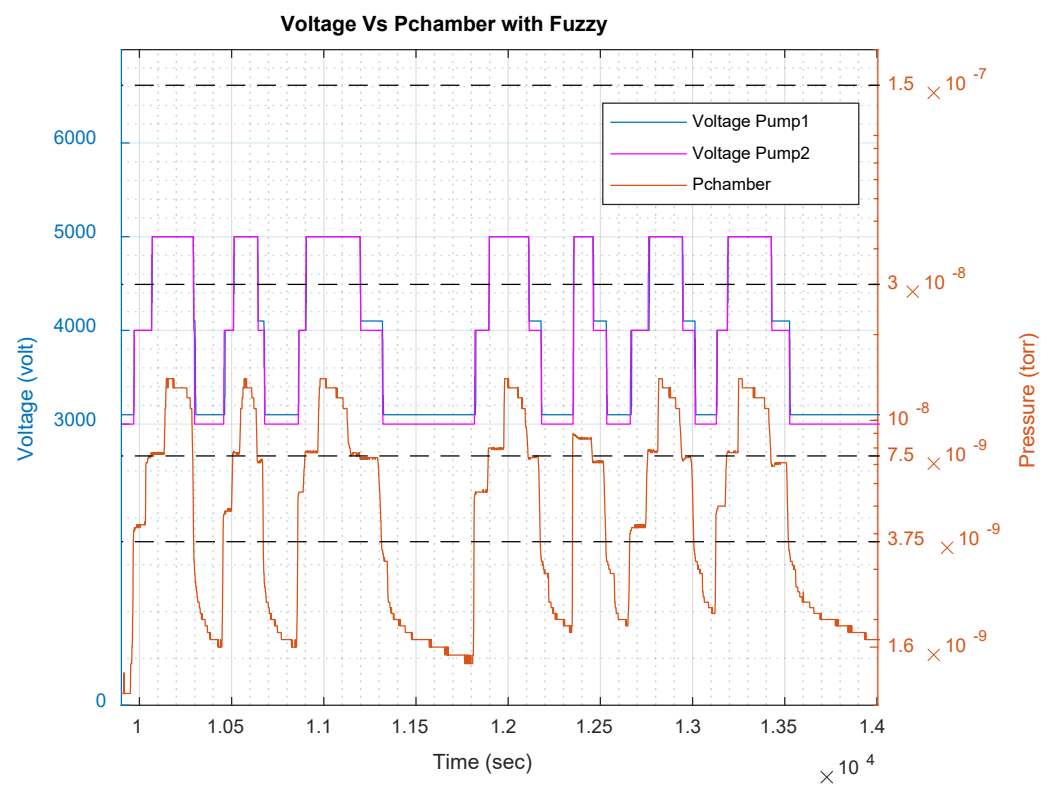


Figure 17. The control results for system 2.

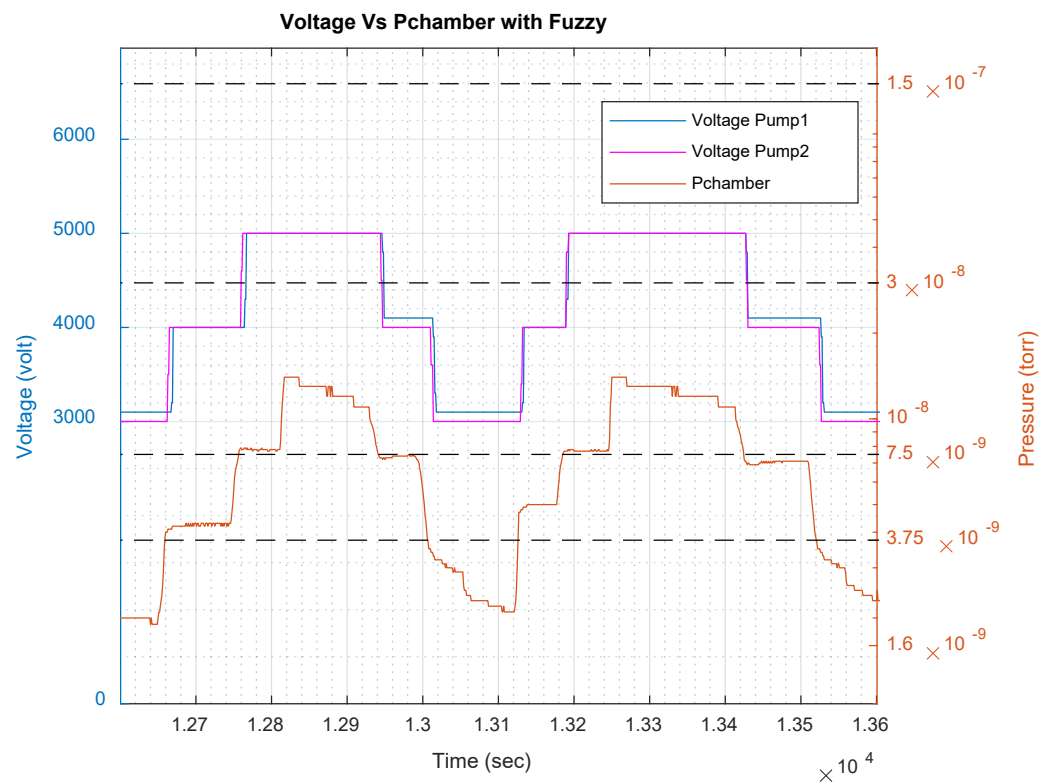


Figure 18. The control results expanded for clarity of the system 2.

4. Pumping Speed Efficiency Estimation

The pumping speed efficiency is an indicator for assessing the capacity of a vacuum pressure system. If the pump has poor performance, it will negatively impact the results of the vacuum chamber pressure. Therefore, understanding the performance of the pump is essential for planning to achieve the desired pressure. In this section, we will apply the use of Molflow+ and artificial neural network (ANN) to predict pump speed efficiency.

4.1. MolFlow+

Molflow+ is free software copyrighted by CERN and E.S.R.F., and it is a Windows program that calculates the steady-state pressure in complex geometries under UHV conditions. The simulation process typically involves four steps: importing the geometry; setting simulation parameters, such as temperature and reflective properties; defining outgassing and pump locations; and viewing pressure profiles [41]. It is gaining attention from the scientific community for its ability to perform detailed 3D calculations of vacuum in the molecular flow regime. The software is discussed in relation to vacuum calculation methods, and examples of its application in the design and analysis of vacuum systems at CERN and elsewhere are presented [42]. The steady-state and time-dependent algorithms behind the program are also discussed, along with strategies for addressing common issues that arise when simulating large systems. The results are compared to the theory and validated through experiments.

In this study, the Molflow+ software was utilized to analyze the behavior of vacuum pressure in an experimental system. The process involved determining the outgassing rate by setting a pumping speed of 288 l/s and measuring pressure values in millibars. The results were then compared with pump efficiency at different percentages of outgassing rate, as shown in Table 6.

Table 6. Pumping performance at a speed of 288 L/s for a vacuum chamber experimental system 1.

%Outgassing Rate	Q (mbar. L/s)	Pc (mbar)	Pi (mbar)
−15%	2.975×10^{-11}	2.55×10^{-10}	1.97×10^{-10}
−10%	3.15×10^{-11}	2.70×10^{-10}	2.09×10^{-10}
−5%	3.325×10^{-11}	2.86×10^{-10}	2.21×10^{-10}
normal	3.5×10^{-11}	3×10^{-10}	2.32×10^{-10}
5%	3.675×10^{-11}	3.15×10^{-10}	2.44×10^{-10}
10%	3.85×10^{-11}	3.31×10^{-10}	2.56×10^{-10}
15%	4.025×10^{-11}	3.45×10^{-10}	2.67×10^{-10}

The results from Table 6 indicate that when the pumping speed is held constant, an increase in the outgassing rate leads to higher pressure in the vacuum pump (Pi) and the measuring device (Pc) attached to it. This aligns with the theory that the outgassing rate is the rate at which gas is removed from the system, thereby reducing the pressure. Factors, such as the permeability of the material surface, also play a role in this process. The more gas particles are removed, the higher the pressure will be. On the other hand, when the pumping speed is constant, a decrease in the outgassing rate leads to a lower pressure in the system, creating a higher vacuum at both the vacuum pump and the measuring instrument’s positions.

Molflow+ software is utilized to visualize the behavior of vacuum pressure in an experimental system. The software displays the vacuum pressure values along individual color axes generated within the system, with the distance being represented as 0–100% of the axis of each plane. The simulation results of pressure values are separated into two experimental systems: vacuum chamber system 1; and the system connected between vacuum chamber 1 and vacuum chamber 2 by pipes. These systems have an inner diameter of 60.3 mm and a length of 1000 mm.

The vacuum chamber 1 has a diameter of 152.4 mm and a height of 285 mm, with a total volume, including the flange, of 4,498,615.15 mm³. The red axial pressure value is measured from the position of the sputter-ion vacuum pump to the cover of the top flange, with a length equal to the height of 285 mm. The green axis, from the CF 70 flange position to the edge of the vacuum chamber, is 194 mm long. The blue axis, from the flange position CF 70 to CF 114, is 273 mm long. These values are shown in Figure 19, and the vacuum pressure values at each position of each axis are shown in Table 7.

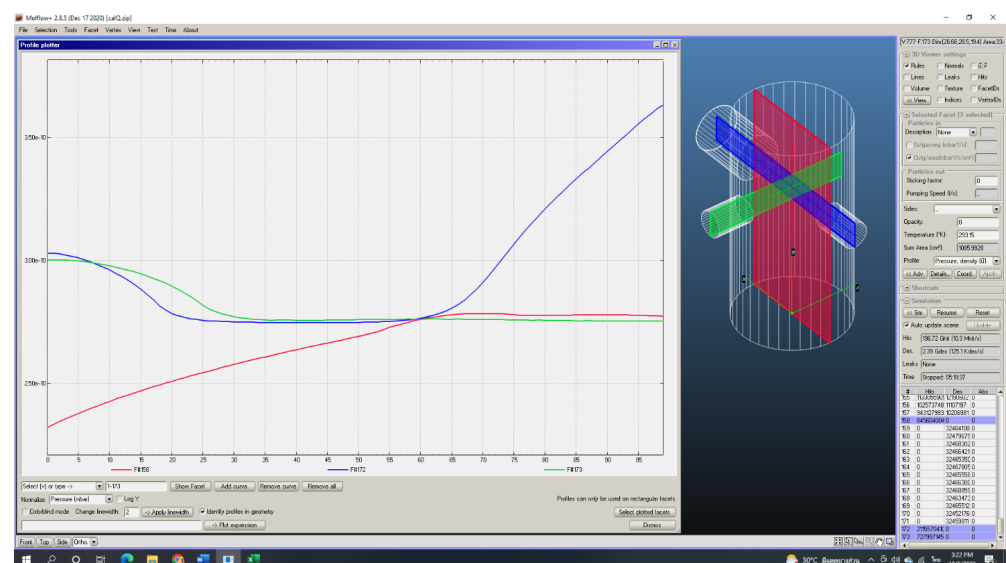


Figure 19. The axial pressure in vacuum chamber 1 with the Molflow+ software.

Table 7. The vacuum pressure in the vacuum chamber 1 from Molflow+ software.

%x	Red Line Axial Pressure		Green Line Axial Pressure		Blue Line Axial Pressure	
	x (mm)	P (10^{-10} Mbar)	x (mm)	P (10^{-10} Mbar)	x (mm)	P (10^{-10} Mbar)
0	0	2.32	0.00	3	0.00	3.03
0.05	14.25	2.38	9.70	3	13.65	3.01
0.10	28.50	2.43	19.40	2.98	27.30	2.96
0.15	42.75	2.47	29.10	2.95	40.95	2.89
0.20	57.00	2.51	38.80	2.9	54.60	2.79
0.25	71.25	2.55	48.50	2.82	68.25	2.76
0.30	85.50	2.58	58.20	2.77	81.90	2.75
0.35	99.75	2.61	67.90	2.76	95.55	2.75
0.40	114.00	2.64	77.60	2.76	109.20	2.75
0.45	128.25	2.67	87.30	2.76	122.85	2.75
0.50	142.50	2.69	97.00	2.76	136.50	2.75
0.55	156.75	2.73	106.70	2.76	150.15	2.75
0.60	171.00	2.76	116.40	2.76	163.80	2.77
0.65	185.25	2.78	126.10	2.76	177.45	2.81
0.70	199.50	2.78	135.80	2.76	191.10	2.91
0.75	213.75	2.78	145.50	2.76	204.75	3.07
0.80	228.00	2.78	155.20	2.76	218.40	3.21
0.85	242.25	2.78	164.90	2.76	232.05	3.33
0.90	256.50	2.78	174.60	2.76	245.70	3.45
0.95	270.75	2.78	184.30	2.76	259.35	3.56
1.00	285.00	2.78	194.00	2.76	273.00	3.63

According to Table 7, the red line represents the height of the chamber, the green line represents the diameter distance, and the blue line represents another diameter distance. The intersection of the three colored lines represents a vacuum pressure of 2.76×10^{-10} mbar at the position indicated in the red frame. The data from the simulation, which uses values measured by sensors in the $x = 0$ mm position of the green and red lines from the experiment, serves as reference values to simulate the outgassing rate over the entire surface of the gas vacuum chamber 1. This outgassing rate was found to be 3.5×10^{-11} mbar.L/s when the pumping rate was set to 288 L/s. This value aligns with the equation that displays the relationship between vacuum pressure values at 3000 V, as shown in Table 3.

In this research, an experimental vacuum system was constructed, consisting of two vacuum chambers (1 and 2) connected by a tube. The dimensions of chamber 2 are 152.4 mm in diameter, 310 mm in height, and a total flange volume of 5,248,639.03 mm³. The tube connecting the chambers has an outer diameter of 65 mm, an inner diameter of 60.3 mm, and a length of 1000 mm (as shown in Figure 20). The vacuum pressure values in each axis show the relationship between the values measured from the position of the instrument. Measurements A, B, C, and D are represented by the blue, green, red, and black lines, respectively. The pumping speed of each pump was determined by substituting the pressure pumped by the pump into the pressure source equation (shown in Table 2). This allowed for the determination of the outgassing rate of each system. By comparing the simulation data with the measurement data from the combined vacuum pressure instrument, it was determined that the starting point in the blue and red axis is the location of the pump, which has the best vacuum pressure value. The pressure continues to increase axially to the upper cover of vacuum chambers 1 and 2. The black line axis shows the pressure at the location where sensor D is installed, while the green line axis shows the pressure along the length of the pipe connecting the two vacuum chambers. The center of the pipe at sensor B has the highest pressure in the system, at which point the researchers used to control the pressure to a UHV to confirm pressure values in other locations. This ensured that there was also a UHV pressure value.

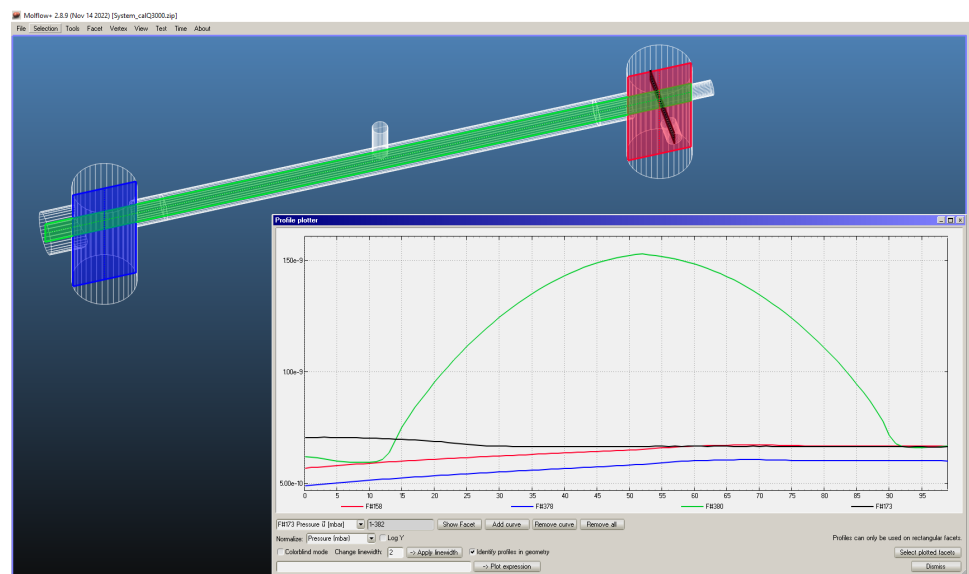


Figure 20. The profile pressure in vacuum system with the Molflow+ software.

The next step is to apply the information obtained from the vacuum pressure simulation in the Molflow+ program using an artificial neural network to find the model of the vacuum system that has been created. The process begins by using fuzzy control to adjust the voltage supply to the sputter-ion pump in order to optimize the pumping speed within a specific pressure range. Data on pressure at various locations is collected using a measuring device, and the pumping speed is calculated from the actual measured pressure. The situation is then simulated using the Molflow+ program to obtain data on the outgassing rate of the system. The process is iterated until a sufficient data set is obtained for learning through the neural network to model the vacuum experimental system. This step will also allow for the determination of the pumping speed efficiency of the pump, which will be discussed in the next section.

4.2. Artificial Neural Network (ANN)

Machine learning is a powerful technique that is used to solve several problems in the engineering field. Computational technology is rapidly growing in both hardware and software architectures which allows machine learning to be applied to complicated works. An artificial neural network is an efficient algorithm of machine learning that is utilized for outgassing prediction in the UHV pressure control system. Supervise learning neural network based on a multivariable regression approach was utilized to tackle prediction model training. Moreover, this research has been focusing on the effect of various network structures that need to be optimized to achieve the desired performance of the prediction model. To develop the purpose neural network model, it would be addressed at each step, as shown in Figure 21.

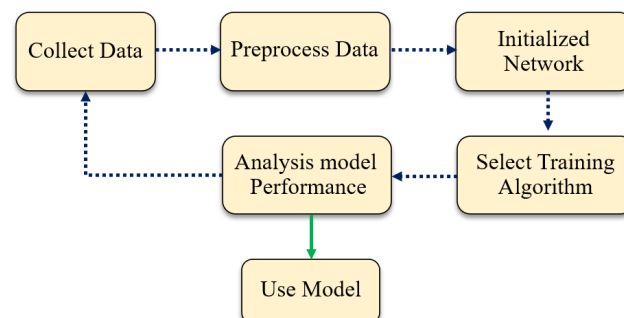


Figure 21. Neural Network Training Process Flow.

4.2.1. Data Collection and Preprocessing

To investigate outgassing and pumping speed prediction, the training data set was collected based on simulation software. The process to generate the training data set was performed by using the data from a Molflow+ simulation to train a neural network that predicts the pumping speed of ion pumps and outgassing rates in different parts of a system. The system is divided into three sections: the first vacuum chamber (Qa); the conduit between two vacuum chambers (Qb); and the second vacuum chamber (Qc). The neural network is trained using data collected at steady-state intervals to test for changes in pumping speed and outgassing rates and verified by the Molflow+ program. The inputs used for the prediction are pressure values from different parts of the measuring instrument in the experimental system (Pa, Pb, Pc, Pd, Ppump1, and Ppump2), and the outputs are the pumping speed (Spump 1, Spump 2) and outgassing rates (Qa, Qb, and Qc). Data preprocesses. All cases have been arranged into a matrix of input and output which overall have 90 samples. To evaluate model performance during the network learning process, it needs to divide the data into three sections for training, validation, and testing, accounting for 70%, 15%, and 15%, respectively. To handle the complicated relation of input and output data, the model would be separated into the independent model for outgassing and pumping speed prediction, as shown in Figure 22.

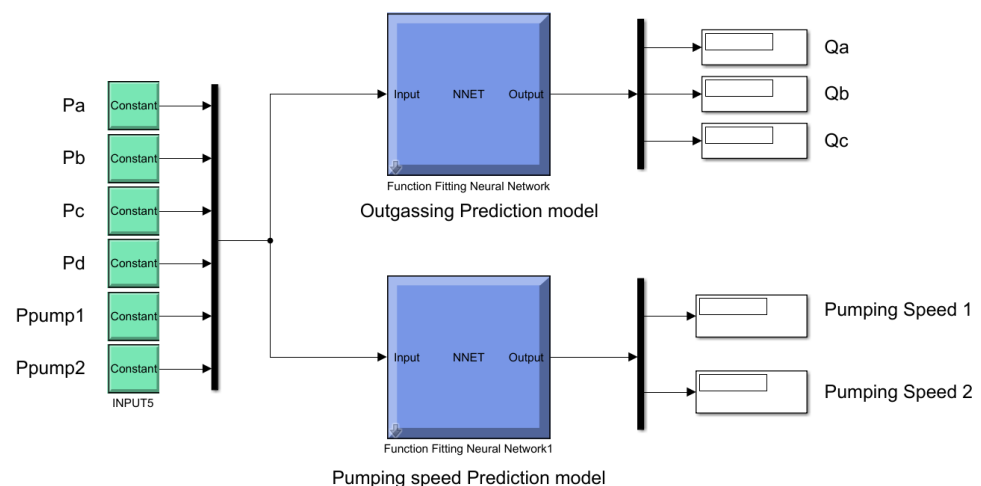


Figure 22. Independent model for Outgassing and pumping speed prediction.

4.2.2. Select Architecture and Training the Network

The development of the neural network could be addressed in varying implementations, which can consider three major categories, including classification, prediction, and regression model. In this work, we provided the multilayer network architecture that was performed in a regression task used to approximate a function of input corresponding to the continuous output from the model. In general, there are various factors to take into consideration for a good network depending on the complex relation of data and area of application. One of the most common techniques that are possible to examine network performance is changing of hidden layer size and neural number in each layer. Moreover, the learning algorithms are the crucial points that need to be regarded to optimize the weight and bias of the network. The Scale Conjugate Gradient (Trainscg) is a potential algorithm for regression that incorporate to the Linear Transfer function (purelin) in each neural node of the model. The configuration of the network on the MATLAB program (MATLAB 2020b License No. 199467, Suranaree University of Technology) was displayed in Figure 23.

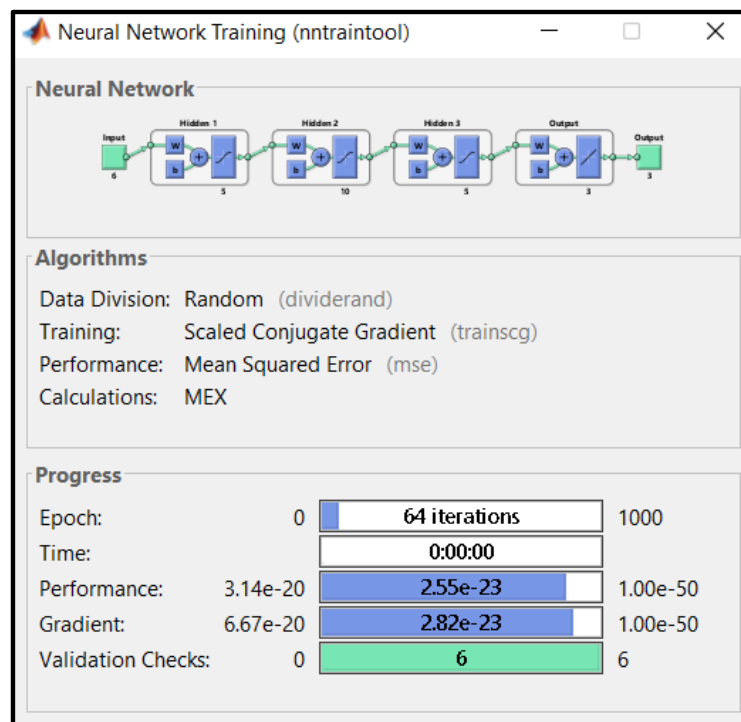


Figure 23. MATLAB program pretraining configuration.

The training part is performed to allow the network to adjust its weight and bias parameter corresponding to the error between the estimated output and the target. The random initializing of weight and bias caused the difference of result in training; by this reason it needed to be retrained beneficial to capture the best network model. As the result, Figure 24 indicated the performance curve based on Mean Square Error (MSE) cost function of the outgassing and pumping speed prediction model.

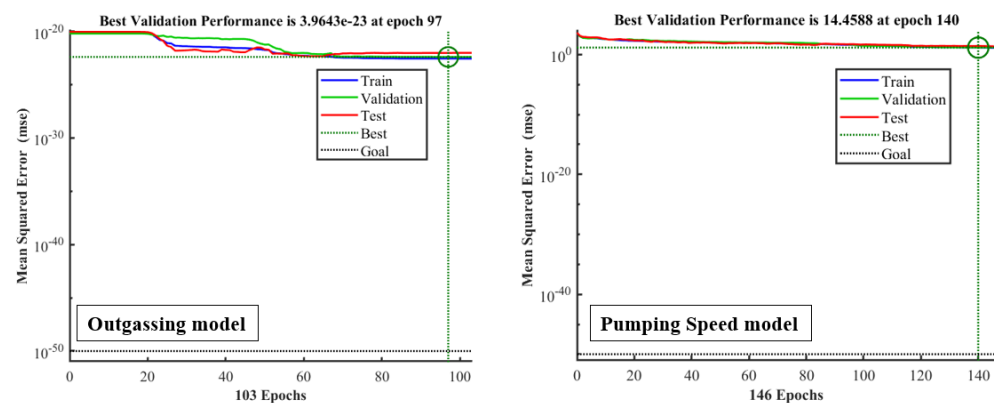


Figure 24. MSE of Outgassing and Pumping speed model.

The two performance graphs displayed the minimizing of MSE over the training iteration (Epochs). The minimum value of MSE would be the best network model; meanwhile, it needs the validation check in each epoch to manipulate an overfitting phenomenon. The experiment revealed that the optimal network of outgassing and pumping speed model is verified MSE representing 3.9643×10^{-23} at 97 epochs and a14.4588 at 140 epochs. Implementation of the regression network model must be evaluated using the R^2 . For perfect function approximation are given $R^2 = 1$; however, there are many uncertainties that affect this value, for instance, outlier, missing value, and amount of data point. Figure 25 illustrates the recession result in R^2 at the best validation point, which is displayed as 0.99851 for

outgassing and 0.99234 for the pumping speed model. It is implied that the network model can be used to predict the output in a limitation of supervising data set. The analysis result will be validated with actual experiment data. Consequently, the appropriated network can apply to the control system, which leads to increased reliability of the UHV process.

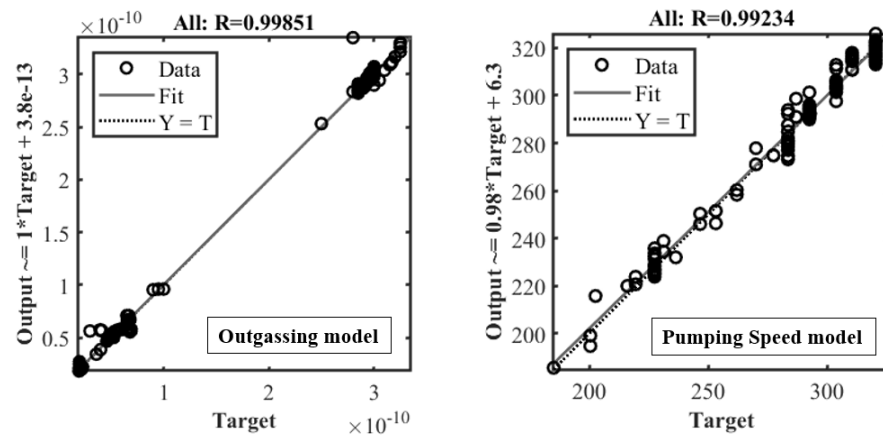


Figure 25. R² of Outgassing and Pumping speed model.

4.2.3. Analysis of Estimation Model Performance

Table 8 displays the steady-state pressure values for the measuring instruments from four experiments, along with the predicted outgassing results from the neural network. These predicted values are further validated by Molflow+ simulation. The correlation between the obtained values and the measurement data can be seen in Table 9.

Table 8. The prediction of outgassing by an ANN from the pressure measurement experiment.

Data Measuring from an Instrument of the Experimental					Outgassing Prediction from ANN			
Pa	Pb	Pc	Pd	Ppump1	Ppump2	Qa	Qb	Qc
9.0659×10^{-10}	1.8665×10^{-9}	2.2665×10^{-9}	2.5331×10^{-9}	5.8662×10^{-10}	1.7332×10^{-9}	5.89×10^{-11}	2.63×10^{-11}	3.13×10^{-10}
8.3993×10^{-10}	1.7332×10^{-9}	2.2665×10^{-9}	2.3998×10^{-9}	6.1328×10^{-10}	1.7332×10^{-9}	5.83×10^{-11}	2.24×10^{-11}	3.11×10^{-10}
1.0399×10^{-9}	1.8665×10^{-9}	2.3998×10^{-9}	2.5331×10^{-9}	5.0662×10^{-10}	1.8665×10^{-9}	5.88×10^{-11}	2.43×10^{-11}	3.05×10^{-10}
9.1992×10^{-10}	1.8665×10^{-9}	2.2665×10^{-9}	2.5331×10^{-9}	6.5328×10^{-10}	1.7332×10^{-9}	5.97×10^{-11}	2.84×10^{-11}	3.11×10^{-10}

Table 9. The comparison result between prediction and experiment.

Experimental Results for Determining the Pumping Speed and Root Mean Square Error					
Calculation		ANN		RMSE	
Spump1	Spump2	Spump1	Spump2	Ppump1	Ppump2
312.34	342.26	253.33	266.00	9.84804×10^{-22}	7.53585×10^{-21}
313.56	342.26	242.81	272.79	5.95539×10^{-23}	2.82551×10^{-22}
308.29	344.31	249.88	268.52	1.15294×10^{-20}	1.35753×10^{-20}
315.31	342.26	239.84	273.63	5.96047×10^{-23}	1.35492×10^{-21}

From experimental Table 9, data from four measurements were collected and used to calculate the pumping speed. The table on the left displays the results calculated from the equation, the middle shows the results obtained from the neural network method, and the right displays the calculation of the root mean square error for each data. During the experiment, there were two sputter-ion pumps. Firstly, the values of pumping speed 1 and pumping speed 2 calculated via the equation were 312.34 and 342.26, respectively, while the values obtained via the artificial neural network method were 253.33 and 266.00. The corresponding root mean square errors were 9.84804×10^{-22} and 7.53585×10^{-21} , respectively. Secondly, the values for pumping speed 1 and pumping speed 2 calculated via the equation were 313.56 and 342.26, respectively, while the values obtained via the neural

network method were 242.81 and 272.79. The corresponding root mean square errors were 5.95539×10^{-23} and 2.82551×10^{-22} , respectively. Thirdly, the values of pumping speed 1 and pumping speed 2 calculated via the equation were 308.29 and 344.31, respectively, while the values obtained via the neural network method were 249.88 and 268.52. The corresponding root mean square errors were 1.15294×10^{-20} and 1.35753×10^{-20} , respectively. Lastly, the values for pumping speed 1 and pumping speed 2 calculated via the equation were 315.31 and 342.26, respectively, while the values obtained via the neural network method were 239.84 and 273.63. The corresponding root mean square errors were 5.96047×10^{-23} and 1.35492×10^{-21} , respectively. Upon considering the root mean square error, it was found that the values were very small. Furthermore, when considering the increase and decrease of the pumping speed, it tends to go in the same trend.

5. Conclusions

Synchrotron light production requires advanced vacuum technology to stabilize and prevent electron interference in a UHV pressure environment of about 10^{-9} Torr, which may affect the quality of light. To achieve this, a vacuum pressure system is created, and leak detection is performed. A fuzzy controller design is used in UHV systems to measure pressure from the instrument in a steady state. The Molflow+ program is used to simulate the outgassing rate of the system and feed it into the learning process of a neural network to create a model of the UHV system. Since current mathematical models are insufficient and complicated for estimation in all situations, an artificial neural network is used to simulate a mathematical model that aligns with experimental results.

The experimental results revealed the steady state pressure at the location where the measuring instrument was installed. The pressure obtained from the test corresponds to the pumping speed equation, but it cannot determine the outgassing rate of the system. To determine the outgassing rate, Molflow+ simulations are used. The simulation results are then used in neural network learning to model the vacuum system and predict pumping speed performance. The resulting model is validated by comparing the results of the reverse simulation with the Molflow+ program and the actual measurement data. It was found that the obtained values were similar, with RMSE values ranging from 1.3575×10^{-20} to 5.9554×10^{-23} . In this research, the efficiency of the pump was evaluated by utilizing the Molflow+ program in combination with an Artificial Neural Network (ANN). This method enabled suitable UHV control as an alternative to complex mathematical models. The findings can be applied to predict the pump's service life and maintenance planning.

In addition, there are several industries that use UHV systems in their manufacturing or research processes, such as the semiconductor industry; UHV systems are used in the production of semiconductor wafers to create highly precise, defect-free electronic components. The UHV environment helps to prevent contamination and ensure consistent quality throughout the manufacturing process. In the thin film deposition industry, UHV systems are also used in the production of thin films for various applications, such as optical coatings, electronic devices, and solar cells. The UHV environment is necessary to achieve high-quality, uniform deposition of the thin films. In surface science research, UHV systems are used extensively to study the properties of surfaces and interfaces. UHV systems allow researchers to investigate these surfaces without interference from atmospheric gases or contaminants. In all of these industries, the use of fuzzy logic can help to optimize the performance of the UHV system and improve the quality and consistency of the products or research results. By using fuzzy logic to control the various parameters and components of the UHV system, it is possible to achieve highly precise and efficient operation, leading to better results and reduced costs, as well as reducing the risk of human error.

Author Contributions: Conceptualization, S.S. and J.S.; methodology and validation, S.S., N.K. and J.S.; software and formal analysis, S.S., N.Y., T.W. and J.S.; experimental setup and data collection, S.S. and J.S.; investigation, J.S.; writing—original draft preparation, S.S.; writing—review and editing, S.S., T.W., N.K. and J.S. All authors have read and agreed to the published version of the manuscript.

Funding: This research was funded by Synchrotron Light Research Institute (Public Organization). It offers a scholarship for Students at the Suranaree University of Technology (SUT) agency through grant number PHD5940301.

Data Availability Statement: Not applicable.

Acknowledgments: The authors are indebted to Suranaree University of Technology (SUT) and Synchrotron Light Research Institute (Thailand) for their generosity, budgets, equipment, locations, and valuable comments.

Conflicts of Interest: The authors declare no conflict of interest.

References

1. Sujitjorn, S. Thai Synchrotron Facility: It's Past and Present. *Suranaree J. Sci. Technol.* **2015**, *22*, 227–230.
2. Grabski, M. *Vacuum Technology for Particle Accelerators*; Introduction to Accelerator Physics; CERN Accelerator School: Budapest, Hungary, 2016.
3. Li, Y.; Liu, X. *Vacuum Systems Engineering*; Vacuum Science and Technology for Accelerator Vacuum Systems; Cornell University: Ithaca, NY, USA, 2015.
4. Akram, H.M. Selection of Precise Vacuum Pumps for Systems with Diverse Vacuum Ranges. *Glob. J. Res. Eng.* **2014**, *14*, 645–651.
5. Bertolini, L. Ion Pumps. Presented at The U.S. Particle Accelerator School, Lawrence Livermore National Laboratory, 10–14 June 2002. Available online: https://uspas.fnal.gov/materials/02Yale/05_IonPumps.pdf (accessed on 1 January 2023).
6. Polozov, S.; Dyubkov, V.; Panishev, A.; Shatokhin, V. Vacuum Condition Simulations for Vacuum Chambers of Synchrotron Radiation Source. In Proceedings of the 27th Russian Particle Accelerator Conference, Alushta, Russia, 27 September–1 October 2021. [CrossRef]
7. Dong, C.; Mehrotra, P.; Myneni, G.R. *Several Technical Measures to Improve Ultra-High and Extreme-High Vacuum*; UNT Libraries Government Documents Department: Denton, TX, USA, 2002; pp. 1–6.
8. Suetsugu, Y. *Numerical Calculation of an Ion Pump's Pumping Speed*; Elsevier Ltd.: Amsterdam, The Netherlands, 1995; Volume 46, pp. 105–111.
9. Geng, J.; Wang, X.; Guo, M.; Zhang, S.; Cheng, Y.; Li, Y.; Li, H.; Ren, Z. Research on Measuring Method of Pumping Speed for Miniature Sputter Ion Pump. *Measurement* **2022**, *190*, 110736. [CrossRef]
10. Dolcino, L.; Mura, M.; Paolini, C. *50 Years of Varian Sputter Ion Pumps and New Technologies*; Elsevier Ltd.: Amsterdam, The Netherlands, 2010; Volume 84, pp. 677–684.
11. Tsipenyuk, D.Y. *Vacuum Technology. Physical Methods, Instruments, and Measurements*; Russian Academy of Sciences: Moscow, Russia, 2009; Volume 3, pp. 305–326. ISBN 978-1-905839-56-8.
12. Calcatelli, A.; Bergoglio, M.; Mohan, P.; Spagnol, M.; Simon, M.D. *Study of Outgassing of Sputter-Ion Pump Materials Treated with Three Different Cleaning Procedures*; Elsevier Ltd.: Amsterdam, The Netherlands, 1996; Volume 47, pp. 723–726.
13. Ady, M. Monte Carlo Simulations of Ultra High Vacuum and Synchrotron Radiation for Particle Accelerators. Ph.D. Thesis, École Polytechnique Fédérale de Lausanne, Lausanne, Switzerland, 2016.
14. Wang, G.; Zhang, S.; Chen, C.; Tang, N.; Lang, J.; Xie, Y. Vacuum System Optimization for EAST Neutral Beam Injector. *Energies* **2022**, *15*, 264. [CrossRef]
15. Shen, S.; Tung, L.; Kishiyama, K.; Nederbragt, W. Design and Analysis of Vacuum Pumping Systems for Spallation Neutron Source Drift-Tube Linac and Coupled-Cavity Linac. In Proceedings of the 2001 Particle Accelerator Conference, Chicago, IL, USA, 18–22 June 2001.
16. Odnagam, S.; Preecha, C.; Sanwong, P.; Thongtan, W.; Srisertpol, J. Precision Analysis and Design of Rotating Coil Magnetic Measurements System. *Appl. Sci.* **2020**, *10*, 8454. [CrossRef]
17. Prawanta, S.; Srisertpol, J. Plane Stabilization of the Electron Storage Ring Using Automatic 3-DOF Girder System. *Int. J. Mech. Mechatron. Eng.* **2018**, *18*, 35–44.
18. Yachum, N.; Chunjarean, S.; Russamee, N.; Srisertpol, J. Parameter Optimization of Hole-Slot-Type Magnetron for Controlling Resonant Frequency of Linear Accelerator 6 MeV by Reverse Engineering Technique. *Appl. Sci.* **2021**, *11*, 2384. [CrossRef]
19. Nguyen, H.T.; Prasad, N.R.; Walker, C.L.; Walker, E.A. *A First Course in Fuzzy and Neural Control*, 1st ed.; Chapman and Hall/CRC: Boca Raton, FL, USA, 2002. [CrossRef]
20. Ibrahim, A.M. Fuzzy Logic for Embedded Systems Applications. In *Fuzzy Logic for Embedded Systems Applications*, 1st ed.; Elsevier: Amsterdam, The Netherlands, 2003; ISBN 9780080469904.
21. Wu, H.N.; Reliable, L.Q. Fuzzy Control for Continuous-Time Nonlinear Systems with Actuator Faults. *IEEE Trans. Syst. Man Cybern. Part B Cybern.* **2004**, *34*, 1743–1752. [CrossRef] [PubMed]

22. Somwanshi, D.; Bundeale, M.; Kumar, G.; Parashar, G. Comparison of Fuzzy-PID and PID Controller for Speed Control of DC Motor Using LabVIEW. *Procedia Comput. Sci.* **2019**, *152*, 252–260. [[CrossRef](#)]
23. Ma, F. An Improved Fuzzy PID Control Algorithm Applied in Liquid Mixing System. In Proceedings of the 2014 IEEE International Conference on Information and Automation (ICIA), IEEE, Hailar, China, 28–30 July 2014; pp. 587–591. [[CrossRef](#)]
24. Srisertpol, J.; Numanoy, N.; Pewmaikam, C. PI Controller plus Adaptive Fuzzy Logic Compensator for Torque Controlled System of DC Motor. In Proceedings of the 3rd International Conference on Engineering and Applied Science (2013 ICEAS), Osaka, Japan, 7–9 November 2013.
25. Patel, H.R.; Shah, V.A. Fuzzy Logic Based Metaheuristic Algorithm for Optimization of Type-1 Fuzzy Controller: Fault-Tolerant Control for Nonlinear System with Actuator Fault. *IFAC-PapersOnLine* **2022**, *55*, 715–721. [[CrossRef](#)]
26. Tan, J.H.; Tan, T.S.; Chia Hiik, K.L.; Mat Saad, A.Z.; Malik, S.A. Two-N Input Output Mapping Relationship Fuzziness Adaptation Approach for Fuzzy Based Negative Pressure Wound Therapy System. *Expert Syst. Appl.* **2022**, *208*, 118206.
27. Bähr, P.R.; Lang, B.; Ueberholz, P.; Ady, M.; Kersevan, R. Development of a Hardware-Accelerated Simulation Kernel for Ultra-High Vacuum with Nvidia RTX GPUs. *Int. J. High Perform. Comput. Appl.* **2022**, *36*, 141–152. [[CrossRef](#)]
28. Ahmed, S.; Sunil, S.; Mukherjee, S. *A Study on Benchmarking of Molflow for Ultra High Vacuum (UHV) System*; Institute for Plasma Research: Gandhinagar, India, 2020.
29. Carter, J. Design and Analysis of Accelerator Vacuum Systems with SynRad and MolFlow+. Mechanical Engineer, AES-MED Group, Argonne National Laboratory, 2015. Available online: <https://www.aps.anl.gov/files/APS-Uploads/ASDSeminars/2015/2015-09-02-Carter.pdf> (accessed on 1 January 2023).
30. Ady, M.; Kersevan, R. Introduction to the Latest Version of the Test-Particle Monte Carlo Code Molflow. In Proceedings of the IPAC2014: 5th International Particle Accelerator Conference, Beijing, China, 15–20 June 2014; pp. 2348–2350.
31. Rachmatullah, M.I.C.; Santoso, J.; Surendro, K. Determining the number of hidden layer and hidden neuron of neural network for wind speed prediction. *PeerJ Comput. Sci.* **2021**, *7*, e724. [[CrossRef](#)] [[PubMed](#)]
32. Koutsoukas, A.; Monaghan, K.J.; Li, X.; Huan, J. Deep-learning: Investigating deep neural networks hyper-parameters and comparison of performance to shallow methods for modeling bioactivity data. *J. Cheminform.* **2017**, *9*, 42. [[CrossRef](#)] [[PubMed](#)]
33. Yan, Z.; Klochkov, Y.; Xi, L. Improving the Accuracy of a Robot by Using Neural Networks (Neural Compensators and Nonlinear Dynamics). *Robotics* **2022**, *11*, 83. [[CrossRef](#)]
34. Macaulay, M.O.; Shafiee, M. Machine learning techniques for robotic and autonomous inspection of mechanical systems and civil infrastructure. *Auton. Intell. Syst.* **2022**, *2*, 8. [[CrossRef](#)]
35. Lishner, I.; Shtub, A. Using an Artificial Neural Network for Improving the Prediction of Project Duration. *Mathematics* **2022**, *10*, 4189. [[CrossRef](#)]
36. Abdulla, M.B.; Herzallah, R.O.; Hammad, M.A. Pipeline Leak Detection Using Artificial Neural Network: Experimental Study. In Proceedings of the 2013 International Conference on Modelling, Identification and Control, ICMIC, Cairo, Egypt, 31 August–2 September 2013; pp. 328–332.
37. Shen, S.; Lu, H.; Sadoughi, M.; Hu, C.; Nemani, V.; Thelen, A.; Webster, K.; Darr, M.; Sidon, J.; Kenny, S. A physics-informed deep learning approach for bearing fault detection. *Eng. Appl. Artif. Intell.* **2021**, *103*, 104295. [[CrossRef](#)]
38. Castro, O.; Castejón, C.; Garcia-Prada, J.C. Bearing Fault Diagnosis Based on Neural Network Classification and Wavelet Transform. In Proceedings of the 6th WSEAS International Conference on Wavelet Analysis & Multirate Systems, Bucharest, Romania, 16–18 October 2006; Volume 2, pp. 16–18.
39. Zhao, W.; Egusquiza Estévez, E.; Valero Ferrando, M.d.C.; Egusquiza Montagut, M.; Valentín Ruiz, D.; Perras Batlló, A. A Novel Condition Monitoring Methodology Based on Neural Network of Pump-Turbines with Extended Operating Range. In *Proceedings of the 16th IMEKO TC10 Conference on Testing, Diagnostics & Inspection as a Comprehensive Value Chain for Quality & Safety, Berlin, Germany, 3–4 September 2019*; IMEKO: Barcelona, Spain, 2019; pp. 154–159. ISBN 9299008418.
40. Berman, A. *Vacuum Engineering Calculations, Formulas, and Solved Exercises*; Academic Press, Inc.: Cambridge, MA, USA, 1992; ISBN 0120924552.
41. Kersevan, R.; Ady, M. TE-VSC-SCC Training Using Molflow for Sputtering Simulations. CERN, 2020. Available online: https://molflow.web.cern.ch/sites/default/files/scc_training_2020/molflow_for_sputtering.pdf (accessed on 1 January 2023).
42. Ady, M.; Kersevan, R. MolFlow+ User Guide for Version 2.4. CERN. (2014). Available online: https://molflow.web.cern.ch/sites/default/files/molflow_user_guide.pdf (accessed on 1 January 2023).

Disclaimer/Publisher’s Note: The statements, opinions and data contained in all publications are solely those of the individual author(s) and contributor(s) and not of MDPI and/or the editor(s). MDPI and/or the editor(s) disclaim responsibility for any injury to people or property resulting from any ideas, methods, instructions or products referred to in the content.